Available online at www.sciencedirect.com

ScienceDirect

Geochimica et Cosmochimica Acta 214 (2017) 115–142

Geochimica et Cosmochimica Acta

www.elsevier.com/locate/gca

Oxygen isotope fractionation in the $CaCO_3$-DIC-H_2O system

Laurent S. Devriendt [a,*], James M. Watkins [b], Helen V. McGregor [a]

[a] School of Earth and Environmental Sciences, University of Wollongong, NSW 2522, Australia
[b] Department of Earth Sciences, University of Oregon, Eugene, OR, United States

Received 1 December 2016; accepted in revised form 15 June 2017; Available online 4 July 2017

Abstract

The oxygen isotope ratio ($\delta^{18}O$) of inorganic and biogenic carbonates is widely used to reconstruct past environments. However, the oxygen isotope exchange between $CaCO_3$ and H_2O rarely reaches equilibrium and kinetic isotope effects (KIE) commonly complicate paleoclimate reconstructions. We present a comprehensive model of kinetic and equilibrium oxygen isotope fractionation between $CaCO_3$ and water ($\alpha_{c/w}$) that accounts for fractionation between both (a) $CaCO_3$ and the CO_3^{2-} pool ($\alpha_{c/CO_3^{2-}}$), and (b) CO_3^{2-} and water ($\alpha_{CO_3^{2-}/w}$), as a function of temperature, pH, salinity, calcite saturation state (Ω), the residence time of the dissolved inorganic carbon (DIC) in solution, and the activity of the enzyme carbonic anhydrase. The model results suggest that: (1) The equilibrium $\alpha_{c/w}$ is only approached in solutions with low Ω (i.e. close to 1) and low ionic strength such as in the cave system of Devils Hole, Nevada. (2) The sensitivity of $\alpha_{c/w}$ to the solution pH and/or the mineral growth rate depends on the level of isotopic equilibration between the CO_3^{2-} pool and water. When the CO_3^{2-} pool approaches isotopic equilibrium with water, small negative pH and/or growth rate effects on $\alpha_{c/w}$ of about 1–2‰ occur where these parameters covary with Ω. In contrast, isotopic disequilibrium between CO_3^{2-} and water leads to strong (>2‰) positive or negative pH and growth rate effects on $\alpha_{CO_3^{2-}/w}$ (and $\alpha_{c/w}$) due to the isotopic imprint of oxygen atoms derived from HCO_3^-, CO_2, H_2O and/or OH^-. (3) The temperature sensitivity of $\alpha_{c/w}$ originates from the negative effect of temperature on $\alpha_{CO_3^{2-}/w}$ and is expected to deviate from the commonly accepted value (-0.22 ± 0.02‰/°C between 0 and 30 °C; Kim and O'Neil, 1997) when the CO_3^{2-} pool is not in isotopic equilibrium with water. (4) The model suggests that the $\delta^{18}O$ of planktic and benthic foraminifers reflects a quantitative precipitation of DIC in isotopic equilibrium with a high-pH calcifying fluid, leading to a relatively constant foraminifer calcite $\delta^{18}O$-temperature relationship (-0.21 ± 0.01‰/°C). The lower average coral $\delta^{18}O$ data relative to foraminifers and other calcifiers is best explained by the precipitation of internal DIC derived from hydrated CO_2 in a high-pH calcifying fluid and minimal subsequent DIC-H_2O isotopic equilibration. This leads to a reduced and variable coral aragonite $\delta^{18}O$-temperature relationship (-0.11 to -0.22‰/°C). Together, the model presented here reconciles observations of oxygen isotope fractionation over a range of $CaCO_3$-DIC-H_2O systems.

Keywords: Oxygen isotopes; $\delta^{18}O$; Calcite; $CaCO_3$; Kinetic isotope effect; Vital effect; Foraminifera; Coral

1. INTRODUCTION

The equilibrium fractionation of stable oxygen isotopes between carbonate minerals and their host aqueous solution is strongly temperature-dependent (Urey, 1947; McCrea, 1950) making oxygen isotope ratios in marine and terrestrial carbonates the most widely used geochemical proxy for paleo-environment reconstructions (e.g. Emiliani, 1966; Shackleton, 1967; Hays et al., 1976; Winograd et al., 1992; Tudhope et al., 2001; Wang et al., 2001; Siddall et al., 2003). The temperature-dependence of equilibrium isotope partitioning is due to the temperature-dependent bonding properties of the different isotopes (Urey, 1947), and hence

* Corresponding author.
E-mail address: ld404@uowmail.edu.au (L.S. Devriendt).

http://dx.doi.org/10.1016/j.gca.2017.06.022
0016-7037/

equilibrium isotope fractionations are independent of chemical reaction pathways.

In many cases, the isotopic exchange between chemical phases does not reach equilibrium, and mass-dependent transport and reaction rates contribute to the isotopic fractionations. For oxygen isotopes ($^{18}O/^{16}O$) in carbonates, these so-called kinetic isotope effects (KIE) manifest in a variety of ways, including a dependence of oxygen isotopic fractionation on the $CaCO_3$ precipitation rate, the chemical speciation of the dissolved inorganic carbon (DIC; $DIC = CO_{2(aq)} + H_2CO_3 + HCO_3^- + CO_3^{2-}$) and the solution pH (McCrea, 1950; Kim and O'Neil, 1997; Kim et al., 2006; Dietzel et al., 2009; Gabitov et al., 2012; Watkins et al., 2013, 2014). Many natural carbonates grow at rates that likely place them in a non-equilibrium regime and are subject to KIE. To improve interpretations of $\delta^{18}O$ data from modern and fossil carbonates, there is a need to better understand:

(1) Which DIC species contribute to $CaCO_3$ growth?
(2) What controls the isotopic fractionations between the precipitating DIC species and $CaCO_3$?
(3) How does the isotopic composition of DIC species vary prior to and during $CaCO_3$ precipitation?

A recent advance in understanding the controls on oxygen isotope fractionation between precipitating DIC species and $CaCO_3$ (question (2) above) has come from isolating KIE arising from the mineral growth reaction in the presence of the enzyme carbonic anhydrase (CA; Watkins et al., 2013, 2014). CA catalyses the hydration and dehydration of CO_2, thereby increasing the rate of oxygen isotope exchange between the DIC species and H_2O and promoting DIC-H_2O isotopic equilibrium (cf. Uchikawa and Zeebe, 2012). A key result is that in the presence of CA, calcite-water oxygen isotope fractionation is less dependent on the calcite growth rate and solution pH than in calcite growth experiments where the DIC pool is not equilibrated (e.g. Dietzel et al., 2009; Gabitov et al., 2012). This understanding of the KIE between $CaCO_3$ and the precipitating DIC species improves our knowledge of non-equilibrium calcite-water oxygen isotope fractionation but it does not fully explain >2‰ temperature-independent variations in carbonate-water fractionation observed for laboratory grown inorganic $CaCO_3$ (e.g. Kim and O'Neil, 1997; Dietzel et al., 2009; Gabitov et al., 2012) or the cause of oxygen isotope offsets between inorganic and biogenic carbonates (e.g. McConnaughey, 1989a; Spero et al., 1997; Xia et al., 1997; Zeebe, 1999; Adkins et al., 2003; Rollion-Bard et al., 2003; Allison and Finch, 2010a; Ziveri et al., 2012; Hermoso et al., 2016; Devriendt et al., 2017).

In this study, we present a model of oxygen isotope fractionation in the $CaCO_3$-DIC-H_2O system that incorporates the new information on KIE between $CaCO_3$ and DIC (Watkins et al., 2013, 2014), and accounts for the kinetic isotopic fractionations between the DIC and H_2O. In the model, CO_3^{2-} is the only DIC species contributing to carbonate nucleation and growth while other DIC species affect the $^{18}O/^{16}O$ of $CaCO_3$ by conversion to CO_3^{2-} shortly before or during $CaCO_3$ precipitation. The isotopic fractionation between $CaCO_3$ and CO_3^{2-} is calculated as a function of the solution calcite saturation state and ionic strength based on the kinetic expressions of Zhong and Mucci (1993) for calcite precipitation and dissolution. New kinetic isotope fractionations factors (KIFF) associated with the conversions of DIC species are derived based on published experimental data and theoretical calculations. These KIFF are used with published equilibrium isotopic fractionation factors (EIFF, Beck et al., 2005) to calculate the time-dependent isotopic composition of CO_3^{2-} and HCO_3^- as the system relaxes back to an equilibrium state. The model is verified against data from inorganic calcite precipitated from isotopically equilibrated and non-equilibrated DIC pools, and explains the varying effects of calcite growth rate and pH on the calcite-water oxygen isotope fractionation observed in previous studies. Model simulations are also compared to the $^{18}O/^{16}O$ of foraminifers and corals to test current hypotheses of oxygen isotope vital effects in biogenic $CaCO_3$.

2. NOTATION

The $^{18}O/^{16}O$ of a water or carbonate sample ($^{18}R_s$) is measured as the deviation from the $^{18}O/^{16}O$ of a standard ($^{18}R_{std}$) and is expressed using the $\delta^{18}O$ notation:

$$\delta^{18}O_s = \frac{^{18}R_s - {}^{18}R_{std}}{^{18}R_{std}} \times 10^3, \quad (1)$$

where *std* refers to the standard 'Vienna Pee Dee Belemnite' (VPDB) for carbonate samples or 'Vienna Standard Mean Ocean Water' (VSMOW) for water samples. A carbonate $\delta^{18}O$ on the VPDB scale is converted to a $\delta^{18}O$ on the VSMOW scale using the equation provided by Coplen et al. (1983):

$$\delta^{18}O_{VSMOW} = 1.03091\delta^{18}O_{VPDB} + 30.91. \quad (2)$$

The oxygen isotope fractionation factor between any two phases A and B ($\alpha_{A/B}$) is expressed as:

$$\alpha_{A/B} = \frac{^{18}R_A}{^{18}R_B} = \frac{1000 + \delta^{18}O_A}{1000 + \delta^{18}O_B}, \quad (3)$$

where $\delta^{18}O_A$ and $\delta^{18}O_B$ are expressed on the same scale. It is convenient to express the oxygen isotope fractionation factor in ‰ with the term ε:

$$\varepsilon_{A/B} = (\alpha_{A/B} - 1) \times 10^3 \approx \delta^{18}O_A - \delta^{18}O_B. \quad (4)$$

For example, an $\alpha_{A/B}$ value of 1.0295 corresponds to a $\varepsilon_{A/B}$ value of 29.50‰. Hereafter, for phases A or B the following shorthand notation are used: $c = CaCO_3$ and $w = H_2O$.

3. MODEL BACKGROUND

3.1. Contribution of DIC species to $CaCO_3$ growth

For any carbonate oxygen isotope fractionation model, quantifying the relative contribution of DIC species to $CaCO_3$ nucleation and growth is critical because these ions have distinct oxygen isotope ratios (Beck et al., 2005). In

this section, we review current ideas on the relative contribution of CO_3^{2-} and HCO_3^- to $CaCO_3$ nucleation and surface growth.

Several lines of evidence suggest that CO_3^{2-}, rather than HCO_3^-, is the dominant DIC species during $CaCO_3$ nucleation. For example, negligible HCO_3^- concentrations were reported in amorphous calcium carbonate (ACC), the precursor to calcite or aragonite precipitation, suggesting that HCO_3^- ions do not contribute to $CaCO_3$ nucleation (Nebel et al., 2008). Similarly, numerical simulations of calcite (pre-)nucleation, showed that HCO_3^- have a destabilizing effect on the formation of pre-nucleation ACC clusters in solution (Demichelis et al., 2011; Bots et al., 2012). Another clue to the relative contribution of HCO_3^- and CO_3^{2-} ions during carbonate mineral nucleation was inferred from the oxygen isotope ratio of minerals formed quasi-instantaneously following the addition of NaOH in solution (Kim et al., 2006). During these experiments, the rapid precipitation (i.e. negligible back reaction) of a small portion of a DIC pool composed of CO_3^{2-} and HCO_3^- resulted in witherite with $\delta^{18}O$ values reflecting the $^{18}O/^{16}O$ of isotopically equilibrated CO_3^{2-} ions. These results support minimal direct HCO_3^- contribution to carbonate mineral nucleation.

The relative contribution of DIC species to the carbonate mineral during crystal growth following nucleation is less clear. Although there is no direct evidence for HCO_3^- contribution to calcite or aragonite surface growth, the Zuddas and Mucci (1994) kinetic model of calcite growth in seawater and the Wolthers et al. (2012) ion-by-ion model of calcite growth in dilute solution both involve the contribution of HCO_3^- to explain observed mineral growth rate in low pH solutions. However, the importance of HCO_3^- contribution to calcite growth greatly differs between the two models. The Zuddas and Mucci (1994) model suggests that the contribution of HCO_3^- to calcite growth becomes greater than 1% when CO_3^{2-} ions represent less than ~1.5% of the DIC concentration. In contrast, the model of Wolthers et al. (2012) predicts that HCO_3^- adsorption to the growing mineral surface outpaces CO_3^{2-} adsorption for solutions with pH lower than 8.6 (or $[CO_3^{2-}]/[DIC] < 2\%$), representing a contribution of HCO_3^- ions to calcite growth one to two order(s) of magnitude higher than estimates from Zuddas and Mucci (1994). Of note is that Zuddas and Mucci (1994) studied calcite growth kinetics in seawater while Wolters and co-workers derived their model using data from dilute solutions. A solution's ionic strength is known to affect the calcite growth mechanism (Zuddas and Mucci, 1998) and could potentially explain the contrasting modelling results described above. Finally, a significant contribution of HCO_3^- ions to aragonite growth is not supported by oxygen isotopic studies since the $\delta^{18}O$ of aragonite rapidly precipitated from isotopically equilibrated DIC shows no or very little sensitivity to the HCO_3^-/CO_3^{2-} concentration ratio in solution (Kim et al., 2006).

Although future work should clarify the role of HCO_3^- ions during $CaCO_3$ growth, the bulk of evidence suggests no or little contribution of HCO_3^- to calcite/aragonite nucleation and growth. The model presented in this study therefore assumes that $CaCO_3$ precipitates from CO_3^{2-} ions exclusively and that the $\delta^{18}O$ of calcite/aragonite reflects the $^{18}O/^{16}O$ of the carbonate ions consumed during mineral precipitation.

3.2. Models of kinetic isotopic fractionation between $CaCO_3$ and CO_3^{2-} (and HCO_3^-)

Several models have been proposed to explain kinetic oxygen isotope fractionation between $CaCO_3$ and CO_3^{2-} (and HCO_3^-). Watson (2004) and Gabitov et al. (2012) suggested that a competition between calcite surface growth rate and diffusion in the outer monolayers of the crystal determines the net oxygen isotope fractionation between $CaCO_3$ and CO_3^{2-}. This model assumes that the isotopic composition of the mineral surface reflects that of the CO_3^{2-} ions, which are depleted in ^{18}O relative to slowly precipitated $CaCO_3$ (Beck et al., 2005; Kim et al., 2006). The Watson (2004) model relies upon isotopic rearrangement in the ionic bonding environment below the mineral surface, driven by differences in the thermodynamic properties of the mineral surface relative to the bulk lattice. Although the model can reproduce some of the experimental data, it de-emphasizes processes operating on the aqueous side of the solid-fluid interface, such as mass-dependent ion desolvation kinetics, which are likely important (cf. Hofmann et al., 2012; Watkins et al., 2017). Furthermore, the diffusive transport properties of oxygen atoms in calcite at low temperature have not been quantified.

Alternatively, DePaolo (2011) proposed a model that does not require the mineral surface to be in equilibrium with the bulk solution. Instead calcite exchanges oxygen isotopes with the entire DIC pool (i.e. mainly CO_3^{2-} and HCO_3^- because calcite does not grow at low pH) and the fractionation from DIC is controlled by the $CaCO_3$ dissolution/precipitation ratio r_{-c}/r_{+c} (R_b/R_f in DePaolo, 2011). Fractionation varies between an equilibrium limit at $r_{-c}/r_{+c} = 1$ and a kinetic limit at $r_{-c}/r_{+c} = 0$. The r_{-c}/r_{+c} ratio is obtained from calcite dissolution rate estimates and the measured net calcite precipitation rate r_c ($r_c = r_{+c} - r_{-c}$). The r_{-c}/r_{+c} ratio is also invoked in the model of Watkins et al. (2014). However, in the Watkins et al. (2014) model, the contribution of CO_3^{2-} and HCO_3^- to calcite growth is based on an ion-by-ion model of calcite growth (Wolthers et al., 2012) and the r_{-c}/r_{+c} ratio is calculated directly from the solution calcite saturation state rather than from the net growth rate as in the DePaolo (2011) model.

The model presented here follows the same principles as the DePaolo (2011) and Watkins et al. (2014) models in that oxygen isotope fractionation during mineral growth is governed by the $CaCO_3$ dissolution/precipitation ratio. In contrast to the DePaolo (2011) and Watkins et al. (2014) models however, HCO_3^- is not directly involved in calcite growth (Section 3.1). Moreover, a new expression for deriving the $CaCO_3$ dissolution/precipitation ratio is formulated from the Zhong and Mucci (1993) classical crystal growth rate expression (Section 4.2).

3.3. Kinetic isotope fractionations between DIC and H_2O

Understanding DIC-H_2O KIE is critical for interpreting the $\delta^{18}O$ of biogenic $CaCO_3$ (e.g. McConnaughey, 1989b;

Rollion-Bard et al., 2003; Allison and Finch, 2010a; Saenger et al., 2012; Ziveri et al., 2012; Hermoso et al., 2016) and of inorganic $CaCO_3$ precipitating from rapidly dissolving gaseous CO_2 (e.g. Macleod et al., 1991; Clark et al., 1992; Dietzel et al., 1992; Krishnamurthy et al., 2003; Kosednar-Legenstein et al., 2008; Falk et al., 2016) or following CO_2 degassing (e.g. Hendy, 1971; Clark and Lauriol, 1992; Wong and Breecker, 2015).

This study specifically investigates KIE related to CO_2 dissolution. Experiments where calcite was rapidly precipitated in CO_2-fed solutions reported anomalously low calcite-water fractionation factor ($_{c/w}$) relative to that of slowly precipitated inorganic calcite at the same temperature (e.g. Usdowski and Hoefs, 1990; Clark et al., 1992; Dietzel et al., 1992, 2009; Watkins et al., 2013). Under such conditions, $_{c/w}$ is sensitive to the $^{18}O/^{16}O$ of the CO_2 source and strongly decreases with the solution pH (Dietzel et al., 2009). High pH conditions result in strong KIE due to a quasi-unidirectional dissolution and conversion of CO_2 into HCO_3^- and CO_3^{2-} (limited CO_2 degassing), a slow rate of oxygen isotope exchange between DIC species and H_2O (Usdowski et al., 1991), and a fast $CaCO_3$ precipitation rate. Light oxygen isotope enrichments of calcite of 14‰ or more in high pH solutions have been reported in several studies (Clark et al., 1992; Dietzel et al., 2009; Watkins et al., 2013, 2014) and are thought to be caused by (1) the preferential reaction of isotopically light CO_2 molecules with H_2O (hydration) and OH (hydroxylation) following CO_2 dissolution (McConnaughey, 1989b) and (2) the isotopic imprint of oxygen atoms from H_2O and OH into newly formed HCO_3 and CO_3^{2} (Clark et al., 1992). To better understand and accurately predict KIE related to CO_2 dissolution, it is critical to differentiate and quantify (1) and (2). This has not been achieved with experimental data thus far due to uncertainties regarding the level of isotopic re-equilibration between the DIC pool and H_2O prior to calcite precipitation and because KIE between DIC and H_2O could not be isolated from the overall $CaCO_3$-H_2O fractionation factor.

The model presented in this study is used to distinguish and quantify $CaCO_3$-CO_3^{2-} and CO_3^{2-}-H_2O KIE by estimating the level of CO_3^{2-}-H_2O isotopic equilibrium based on solution parameters (Section 4.3). In turn, this permits quantifying the different factors contributing to the observed KIE between DIC and H_2O.

4. MODEL DERIVATIONS

4.1. Model overview

A version of the '^{18}O Carbonate-DIC' (^{18}OCD) model presented here is available as a Microsoft Excel macro at www.LSDevriendt.com. The model integrates oxygen isotopic fractionations arising from the mineral growth reaction and isotopic exchanges between the DIC species and H_2O (Fig. 1). The $CaCO_3$-H_2O fractionation factor $\alpha_{c/w}$ is expressed as:

$$\alpha_{c/w} = \frac{^{18}R_c}{^{18}R_w}. \quad (5)$$

Since CO_3^{2-} is assumed to be the only precipitating DIC species, the numerator and denominator of Eq. (5) are divided by $^{18}R_{CO_3^{2-}}$ (the $^{18}O/^{16}O$ of CO_3^{2-}) to express $\alpha_{c/w}$ as the product of the $CaCO_3$-CO_3^{2-} ($\alpha_{c/CO_3^{2-}}$) and CO_3^{2-}-H_2O ($\alpha_{CO_3^{2-}/w}$) fractionation factors:

$$\alpha_{c/w} = \frac{\frac{^{18}R_c}{^{18}R_{CO_3^{2-}}}}{\frac{^{18}R_w}{^{18}R_{CO_3^{2-}}}} = \alpha_{c/CO_3^{2-}} \cdot \alpha_{CO_3^{2-}/w}. \quad (6)$$

In the model (Fig. 1), the $\delta^{18}O$ of a calcium carbonate mineral ($\delta^{18}O_c$) is calculated from $^{18}R_{CO_3^{2-}}$ and the fractionation factor $\alpha_{c/CO_3^{2-}}$, the latter depending on the degree of isotopic equilibrium between the mineral and the carbonate ion pool (E_c). The fractionation factor $\alpha_{c/CO_3^{2-}}$ reaches an equilibrium limit where $E_c = 1$ while a kinetic (disequilibrium) limit is attained where $E_c = 0$. Here, E_c depends on the $CaCO_3$ precipitation to dissolution reaction rate ratio (DePaolo, 2011), which we infer from the calcite saturation state (Ω) and the solution ionic strength through the partial reaction order for the carbonate ions (n_2).

The $^{18}R_{CO_3^{2-}}$ value (on which $\delta^{18}O_c$ depends) is dependent on the $\delta^{18}O$ of water ($\delta^{18}O_w$) and the fractionation factor $\alpha_{CO_3^{2-}/w}$. The value of $\alpha_{CO_3^{2-}/w}$ also varies between a kinetic and an equilibrium limit. At isotopic equilibrium, $\alpha_{CO_3^{2-}/w}$ only depends on temperature (Beck et al., 2005). Under non-equilibrium conditions, $\alpha_{CO_3^{2-}/w}$ also depends on the $^{18}O/^{16}O$ of the DIC source(s) (e.g. gaseous CO_2), the chemical pathways for the exchange of oxygen isotopes in the DIC-H_2O system and the degree of isotopic equilibrium between the DIC pool and water (E_{DIC}). In turn, E_{DIC} varies between 0 and 1 and is a function of the DIC residence time in solution (calculated from the calcification rate r_c, solution volume V, the DIC concentration [DIC]) and the rate of oxygen isotope exchange between DIC and water (calculated from the solution pH, DIC speciation, temperature and carbonic anhydrase activity CA; Usdowski et al., 1991; Uchikawa and Zeebe, 2012). For example, where calcite forms in a CO_2-fed solution (e.g. Dietzel et al., 2009; Watkins et al., 2013, 2014), the entire DIC pool is derived from hydrated (h_{+2}) and hydroxylated (h_{+4}) CO_2. These reactions initially produce HCO_3^- and CO_3^{2-} ions with distinct $^{18}O/^{16}O$ ratios relative to isotopic equilibrium conditions (McConnaughey, 1989b; Clark et al., 1992; Zeebe, 2014). Over a period of time however, oxygen isotope exchange between the DIC species and water brings $\alpha_{CO_3^{2-}/w}$ towards equilibrium values.

The rates of reactions in the $CaCO_3$-DIC-H_2O system are such that the carbonate ion pool can approach isotopic equilibrium with H_2O ($E_{DIC} \sim 1$) but not with $CaCO_3$ ($E_c < 1$). The opposite scenario of DIC-H_2O isotopic disequilibrium and CO_3^{2-}-$CaCO_3$ equilibrium is unlikely. With respect to oxygen isotopes, the $CaCO_3$-DIC-H_2O system can therefore be in full disequilibrium ($CaCO_3$-CO_3^{2-} and CO_3^{2-}-H_2O disequilibrated), partial equilibrium or disequilibrium ($CaCO_3$-CO_3^{2-} disequilibrated, CO_3^{2-}-H_2O equilibrated) or in full equilibrium ($CaCO_3$-CO_3^{2-} and CO_3^{2-}-H_2O equilibrated). When either part of the system

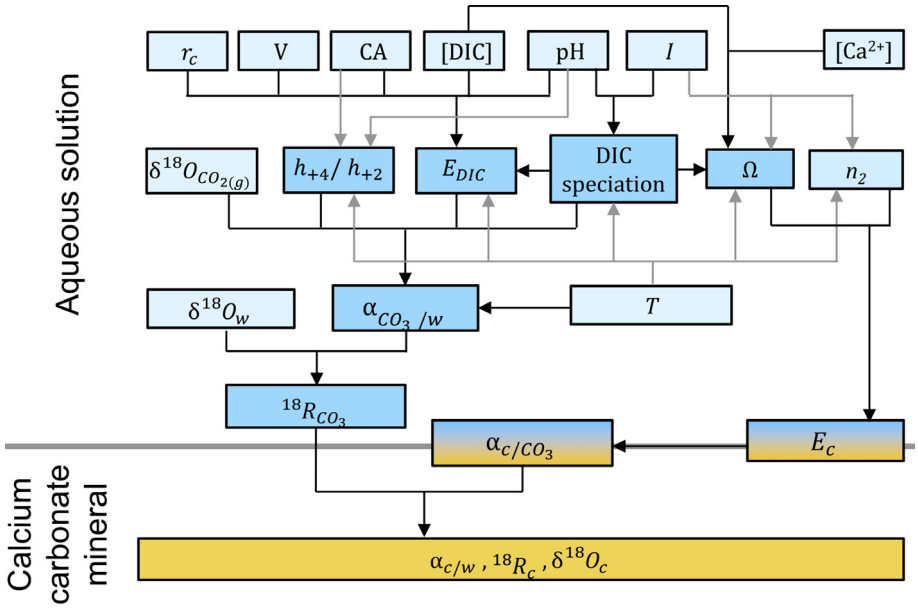

Fig. 1. Factors controlling the $\delta^{18}O$ of inorganic $CaCO_3$ precipitated in a CO_2-fed solution. Model input parameters (light coloured boxes) are used to calculate a set of output parameters (full coloured boxes) upon which the $\delta^{18}O$ of inorganic $CaCO_3$ depends. The arrows indicate the cause and effect relations between the input and output parameters (e.g. Ω is controlled by [Ca^{2+}], [DIC], DIC speciation, salinity and temperature). Where two arrows cross each other, one appears in grey to aid the reading of the flow chart. The subscripts are: "c": $CaCO_3$; "w": water. The symbols and capital letters are: "r_c": $CaCO_3$ precipitation rate (mol/s); "V": volume of precipitating solution (L); "CA": carbonic anhydrase activity (s^{-1}); "[DIC]": DIC concentration (μmol/kg); "I": ionic strength; "[Ca^{2+}]": Ca^{2+} concentration (μmol/kg); "h_{+4}/h_{+2}": CO_2 hydroxylation to hydration reaction rate ratio; "E_{DIC}": isotopic equilibration level between DIC and water (0 to 1); "Ω": calcite or aragonite saturation state (>1); "n_2": partial reaction order with respect to the solution CO_3^{2-} concentration; ^{18}R: $^{18}O/^{16}O$ ratio; α: oxygen isotope fractionation factor; "T": temperature (°C or K); "E_c": level of isotopic equilibration between $CaCO_3$ and CO_3^{2-} (0–1). Where $E_{DIC} = 1$, $\alpha_{CO_3^{2-}/w}$ only depends on temperature and $\alpha_{c/w}$ only depends on temperature and E_c. Where $E_{DIC} < 1$, $\alpha_{CO_3^{2-}/w}$ and $\alpha_{c/w}$ also depend on the $^{18}O/^{16}O$ of the DIC source, E_{DIC}, pH and DIC speciation.

is in disequilibrium then the overall $CaCO_3$-H_2O fractionation should be referred as a disequilibrium fractionation. In Section 4.2, equations for calculating the level of isotopic equilibration between calcite and CO_3^{2-} (E_c) are derived, and then the $\alpha_{c/CO_3^{2-}}$ kinetic (disequilibrium) and equilibrium limits are quantified. Section 4.3 presents equations for calculating the level of isotopic equilibration between CO_3^{2-} and H_2O (E_{DIC}), followed by the quantification of the $\alpha_{CO_3^{2-}/w}$ kinetic and equilibrium limits. Symbols, acronyms and the chemical reactions considered in this study are compiled in Appendices A.1 and A.2 respectively.

4.2. Isotopic fractionation between $CaCO_3$ and CO_3^{2-} ($\alpha_{c/CO_3^{2-}}$)

4.2.1. Kinetic vs equilibrium isotope fractionation

As discussed in Section 3.1, it is assumed that calcite forms via the following reaction pathway:

$$Ca^{2+} + CO_3^{2-} \overset{k_{-c}}{\underset{k_{+c}}{\Longleftrightarrow}} CaCO_3, \tag{7}$$

where k_{-c} and k_{+c} are the backward and forward reaction rate constants, respectively. The isotopic fractionation between a growing mineral and the participating ions in solution was formulated by DePaolo (2011) as a function of the backward/forward reaction rate ratio and is written accordingly for $\alpha_{c/CO_3^{2-}}$:

$$\alpha_{c/CO_3^{2-}} = \frac{\alpha^{+c}_{c/CO_3^{2-}}}{1 + E_c\left(\frac{\alpha^{+c}_{c/CO_3^{2-}}}{\alpha^{eq}_{c/CO_3^{2-}}} - 1\right)}, \tag{8}$$

where $\alpha^{+c}_{c/CO_3^{2-}}$ and $\alpha^{eq}_{c/CO_3^{2-}}$ are the kinetic and equilibrium limits of $\alpha_{c/CO_3^{2-}}$, and E_c is the degree of isotopic equilibrium between $CaCO_3$ and CO_3^{2-}. Where $E_c \approx 0$, $\alpha_{c/CO_3^{2-}}$ approaches $\alpha^{+c}_{c/CO_3^{2-}}$ and where $E_c \approx 1$, $\alpha_{c/CO_3^{2-}}$ approaches $\alpha^{eq}_{c/CO_3^{2-}}$. Following DePaolo (2011) approach, E_c is obtained from the ratio between the backward and forward rate during $CaCO_3$ precipitation:

$$E_c = r_{-c}/r_{+c}, \tag{9}$$

where r_{-c} is the backward (dissolution) rate and r_{+c} is the forward (precipitation) rate. Here we derive a new expression for r_{-c}/r_{+c}, based on the Zhong and Mucci (1993) kinetic model of classic calcite growth. According to the reaction pathway (7), the net reaction rate r_c is expressed as the difference between r_{+c} and r_{-c} (Lasaga, 1981):

$$r_c = r_{+c} - r_{-c} = k_{+c}\{Ca^{2+}\}^{n_1}\{CO_3^{2-}\}^{n_2} - k_{-c}\{CaCO_3\}^{n_3}, \quad (10)$$

where {} denotes ionic or solid activity in the bulk solution and the n_i are the partial reaction rate orders. The activity of solid $CaCO_3$ may be approximated as unity, and if $\{Ca^{2+}\}$ is constant, Eq. (10) can be simplified to (Zhong and Mucci, 1993):

$$r_c = K_{+c}[CO_3^{2-}]^{n_2} - k_{-c} \quad (11)$$

with

$$K_{+c} = k_{+c}\{Ca^{2+}\}^{n_1}\gamma_{CO_3^{2-}}^{n_2}, \quad (12)$$

where [ ] denotes concentration (moles/kg), and $\gamma_{CO_3^{2-}}$ is the activity coefficient of the carbonate ions in solution. At chemical equilibrium, $r_c = 0$, and k_{-c} is expressed as (Zhong and Mucci, 1993):

$$k_{-c} = K_{+c}[CO_3^{2-}]_{(eq)}^{n_2}, \quad (13)$$

where $[CO_3^{2-}]_{(eq)}$ is the concentration of the carbonate ions at chemical equilibrium. Assuming that the backward reaction rate k_{-c} is constant for a given temperature and solute content (i.e., it is independent of Ω, which is akin to 'Model 1' in DePaolo, 2011), the backward and forward reaction rate ratio are expressed as follows:

$$\frac{r_{-c}}{r_{+c}} = \frac{K_{+c}[CO_3^{2-}]_{(eq)}^{n_2}}{K_{+c}[CO_3^{2-}]^{n_2}}. \quad (14)$$

Simplifying Eq. (14) and multiplying the numerator and denominator by $([Ca^{2+}]/K_{sp}^*)^{n2}$, where K_{sp}^* is the stoichiometric solubility product of a $CaCO_3$ mineral (Mucci, 1983, Appendix A.3), yields the following relationship:

$$\frac{r_{-c}}{r_{+c}} = \frac{\left(\frac{[CO_3^{2-}]_{(eq)}[Ca^{2+}]}{K_{sp}^*}\right)^{n_2}}{\left(\frac{[CO_3^{2-}][Ca^{2+}]}{K_{sp}^*}\right)^{n_2}}. \quad (15)$$

Since $[CO_3^{2-}]_{(eq)}$ is the CO_3^{2-} concentration at chemical equilibrium for a given solution (i.e. $[CO_3^{2-}]_{(eq)}$ varies with the solution $[Ca^{2+}]$, temperature and ionic strength), the numerator of Eq. (15) equals 1 regardless of the $[Ca^{2+}]$ value and Eq. (15) simplifies to:

$$\frac{r_{-c}}{r_{+c}} = \Omega^{-n_2} \quad (16)$$

with

$$\Omega = \frac{[CO_3^{2-}][Ca^{2+}]}{K_{sp}^*}. \quad (17)$$

Eq. (16) is a convenient expression for relating r_{-c}/r_{+c} to the saturation state of a carbonate mineral (Ω) and the partial reaction order n_2. The level of isotopic equilibration between $CaCO_3$ and CO_3^{2-} is therefore expected to decrease with increasing solution Ω and n_2. We note, however, that if the mineral reactive surface density (i.e. the kink site density) increases with Ω as expected by some ion-by-ion models of calcite growth (e.g. Nielsen et al., 2012; Wolthers et al., 2012), then the backward rate r_{-c} would also increase with Ω and the level of isotopic equilibration between $CaCO_3$ and CO_3^{2-} would be underestimated at high Ω values.

4.2.2. The partial reaction order n_2

The value of the partial reaction order n_2 is determined by the logarithmic expression of Eq. (11) (Zhong and Mucci, 1993):

$$Log(r_c + k_{-c}) = n_2 Log[CO_3^{2-}] + Log(K_{+c}). \quad (18)$$

When crystal growth is far from chemical equilibrium ($r_c \gg k_{-c}$), Eq. (18) can be approximated by:

$$Log(r_c) = n_2 Log[CO_3^{2-}] + Log(K_{+c}). \quad (19)$$

The partial reaction order n_2 is therefore the slope of $Log(r_c)$ vs $Log[CO_3^{2-}]$ for values of $[CO_3^{2-}]$ far from chemical equilibrium. Experimentally determined n_2 values vary systematically with temperature and ionic strength (Fig. 2A and B; Zuddas and Mucci, 1998; Lopez et al., 2009).

Lopez et al. (2009) derived n_2 for Mg-calcite growing in artificial seawater and NaCa-Cl_2 solution of salinity 35 over the temperature range 5–70 °C. A plot of the Lopez et al. (2009) n_2 values versus temperature (Fig. 2A) shows that n_2 is very similar in seawater and simple NaCa-Cl_2 solutions at a given temperature and that n_2 increases linearly from 2.0 to 3.3 between 0 and 30 °C (Lopez et al., 2009):

$$n_2 = 0.045(\pm 0.002)T\,(^\circ C) + 2.0(\pm 0.1), \text{ for seawater } (I = 0.7) \quad (20)$$

This result is consistent with the findings of several other studies that reported $n_2 \approx 3$ for calcite precipitated in seawater at 25 °C (Zhong and Mucci, 1989, 1993; Zuddas and Mucci, 1994, 1998). The value of n_2 is also strongly dependent on the solution ionic strength, increasing from 0.7 to 3.3 over the 0.1–0.9 range in ionic strength for a solution at 25 °C (Fig. 2B, Zuddas and Mucci, 1998):

$$n_2 = 3.5(\pm 0.6)I + 0.16(\pm 0.37), \quad \text{at } 25\ ^\circ C. \quad (21)$$

Substituting Eq. (20) or (21) into Eq. (16), the level of isotopic equilibrium between calcite and CO_3^{2-} ($E_c = r_{-c}/r_{+c}$) can now be predicted as a function of the solution Ω, temperature and ionic strength. The expected values of E_c at 25 °C as a function of Ω and ionic strength are shown in Fig. 3.

We note that another factor likely to affect n_2 that is not fully covered in this study is the solution CO_3^{2-}/Ca^{2+} activity ratio. At constant Ω, the net calcite growth rate is maximum where the CO_3^{2-}/Ca^{2+} activity ratio is close to 1 and minimum where it is close to 0 or very high (Wolthers et al., 2012). Hence, it can be expected that r_{-c}/r_{+c} also varies with the solution CO_3^{2-}/Ca^{2+}. However, where variations in Ca^{2+} concentration are small and $Ca^{2+} \gg CO_3^{2-}$ (e.g. seawater and most large terrestrial water bodies), Ω is mainly a function of CO_3^{2-} activity and the sensitivity of r_{-c}/r_{+c} (and n_2) to the solution CO_3^{2-}/Ca^{2+} should be small (Wolthers et al., 2012). Hence, we recommend the use of Eqs. (20) and (21) within these specified conditions.

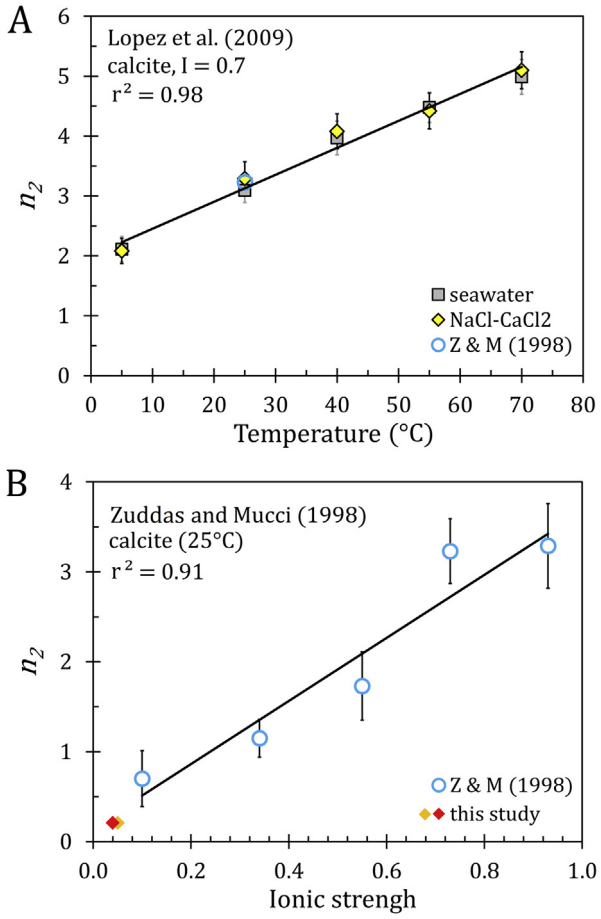

Fig. 2. The effect of temperature and ionic strength on the partial reaction order n_2 for calcite precipitating in seawater and simple NaCl-$CaCl_2$ solutions. (A) Temperature dependence of n_2, data from Zuddas and Mucci (1998) and Lopez et al. (2009). (B) Ionic strength dependence of n_2, data from Zuddas and Mucci (1998). An n_2 value of 0.22 ± 0.02 was estimated for the experimental conditions of Baker (2015) (orange diamond, ionic strength ~ 0.05) and Dietzel et al. (2009) (red diamond, ionic strength ~ 0.03). The parameter n_2 is dependent on the solution temperature and ionic strength, and if these parameters are known, together with the solution Ω, the level of isotopic equilibration between calcite and CO_3^{2-} (E_c) can be calculated.

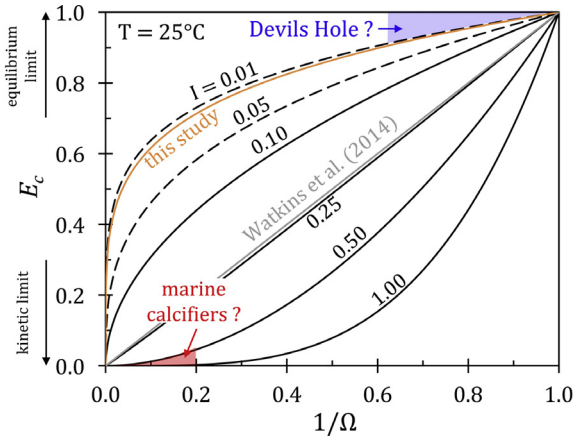

Fig. 3. Modelled isotopic equilibrium level (E_c) between calcite and CO_3^{2-} ($E_c = r_{-c}/r_{+c}$; Eq. (16)) at 25 °C as a function of the solution Ω and for different ionic strengths (I). The lines showing E_c as a function of 1/Ω were calculated using Eqs. (16) and (21). Dotted lines are extrapolations of Eq. (21) for $I < 0.1$. The expectation is that E_c will approach 1 where calcite precipitates at low Ω and low ionic strength (e.g. Devils Hole calcite, $I < 0.01$, $\Omega < 1.6$; Coplen, 2007) and will approach 0 where calcite precipitates at high Ω and high ionic strength (e.g. calcite secreted by marine organisms, $0.5 < I < 1.0$, $\Omega > 5$; Al-Horani et al., 2003; Bentov et al., 2009; de Nooijer et al., 2009; McCulloch et al., 2012; Cai et al., 2016). The oxygen isotope data of Dietzel et al. (2009) and Baker (2015) most closely match the low ionic strength end-member of the model (orange curve, $n_2 = 0.22$, see Section 5.2 and Fig. 7). In comparison, E_c is independent of the ionic strength in the Watkins et al. (2014) model (grey line).

4.2.3. Equilibrium fractionation between $CaCO_3$ and CO_3^{2-}

According to Eq. (6), the oxygen-isotope equilibrium fractionation factor between $CaCO_3$ and CO_3^{2-} ($\alpha^{eq}_{c/CO_3^{2-}}$) is equal to the ratio of the equilibrium fractionation factor between $CaCO_3$ and water ($\alpha^{eq}_{c/w}$) and the equilibrium fractionation factor between CO_3^{2-} and water $\left(\alpha^{eq}_{CO_3^{2-}/w}\right)$:

$$\alpha^{eq}_{c/CO_3^{2-}} = \frac{\alpha^{eq}_{c/w}}{\alpha^{eq}_{CO_3^{2-}/w}}. \quad (22)$$

The true values of $\alpha^{eq}_{c/w}$ for calcite and aragonite have been debated since the pioneering work of Urey (1947). According to Eq. (16), isotopic equilibrium is approached in solutions with low Ω and low ionic strength (Fig. 3). This suggests that the best available estimates of $\alpha^{eq}_{c/w}$ comes from the $\alpha_{c/w}$ of inorganic calcite precipitated very slowly in the low supersaturation and low ionic strength waters of the Devils Hole cave system (see Coplen, 2007; Watkins et al., 2013; Kluge et al., 2014). Using 1.02849 for $\alpha^{eq}_{c/w}$ at 33.7 °C (Coplen, 2007) in Eq. (22), and the expression of Beck et al. (2005) for $\alpha^{eq}_{CO_3^{2-}/w}$ (Table 1), yields an $\alpha^{eq}_{c/CO_3^{2-}}$ of 1.00542 at 33.7 °C. Available data (Dietzel et al., 2009; Baker, 2015, see Section 5.2) suggest that $\alpha_{c/CO_3^{2-}}$ is mostly independent of temperature between 5 and 40 °C, and therefore $\alpha^{eq}_{c/CO_3^{2-}}$ is assumed to be constant. Note that an accurate determination of the temperature sensitivity of $\alpha^{eq}_{c/CO_3^{2-}}$ would require additional oxygen isotope data on inorganic calcite growing at low supersaturation solution (i.e. near equilibrium conditions) and at various temperatures.

4.2.4. Kinetic fractionation between $CaCO_3$ and CO_3^{2-} and between CO_3^{2-} and HCO_3^-

Keeping in mind the framework where only CO_3^{2-} participates directly in calcite growth (pathway (7)), the parameters $^{16}k_{+c}$ and $^{18}k_{+c}$ are defined as rate coefficients of ^{16}O and ^{18}O transfer between carbonate ions and calcite. For the forward reaction, we have (DePaolo, 2011):

$$\frac{^{18}k_{+c}}{^{16}k_{+c}} = \alpha^{+c}_{c/CO_3^{2-}}, \tag{23}$$

where $\alpha^{+c}_{c/CO_3^{2-}}$ is the kinetic limit of $\alpha_{c/CO_3^{2-}}$ during instantaneous calcite precipitation. Under closed system conditions, there are isotopic distillation effects that reduce the kinetic fractionation between product and reactant of a unidirectional reaction (Rayleigh, 1896). In this case, the $^{18}O/^{16}O$ of instantaneously precipitated $CaCO_3$ formed from a finite CO_3^{2-} pool is (Bigeleisen and Wolfsberg, 1958):

$$^{18}R_c = {}^{18}R^{t_1}_{CO_3^{2-}} \frac{1-\left(1-[CO_3^{2-}]_{+c}/[CO_3^{2-}]_{t_1}\right)^{\alpha^{+c}_{c/CO_3^{2-}}}}{[CO_3^{2-}]_{+c}/[CO_3^{2-}]_{t_1}}, \tag{24}$$

where t_1 is the time at the onset of $CaCO_3$ precipitation, $^{18}R^{t_1}_{CO_3^{2-}}$ is $^{18}R_{CO_3^{2-}}$ at t_1, and $[CO_3^{2-}]_{+c}/[CO_3^{2-}]_{t_1}$ is the proportion of CO_3^{2-} consumed during instantaneous $CaCO_3$ precipitation. In cases where $CaCO_3$ precipitation is triggered by a rapid increase in solution pH, all or a fraction of the HCO_3^- ions in solution may be deprotonated and rapidly precipitated. This implies that $^{18}R^{t_1}_{CO_3^{2-}}$ in Eq. (24) can be affected by the initial $^{18}O/^{16}O$ of the HCO_3^- pool and the KIFF related to HCO_3^- deprotonation (Kim et al., 2006). The interconversion of HCO_3^- and CO_3^{2-} occurs via the following pathway:

$$CO_3^{2-} + H^+ \overset{k_{-5}}{\underset{k_{+5}}{\Longleftrightarrow}} HCO_3^-, \tag{25}$$

where k_{-5} and k_{+5} are the reaction rate constants of HCO_3^- deprotonation and CO_3^{2-} protonation, respectively (for the reaction rate constants, we follow the same notation as in Zeebe and Wolf-Gladrow, 2001). Similar to the treatment of the KIFF during CO_3^{2-} precipitation, $^{16}k_{-5}$ and $^{18}k_{-5}$ are defined as rate coefficients of ^{16}O and ^{18}O transfer between bicarbonate and carbonate ions during HCO_3^- deprotonation:

$$\frac{^{18}k_{-5}}{^{16}k_{-5}} = \alpha^{-5}_{CO_3^{2-}/HCO_3^-}. \tag{26}$$

Taking into account distillation effects, the isotopic ratio of the newly formed CO_3^{2-} ions from deprotonated HCO_3^- is (Bigeleisen and Wolfsberg, 1958):

$$R^{-5}_{CO_3^{2-}} = {}^{18}R^{t_0}_{HCO_3^-} \frac{1-\left(1-[CO_3^{2-}]_{-5}/[HCO_3^-]_{t_0}\right)^{\alpha^{-5}_{CO_3^{2-}/HCO_3^-}}}{[CO_3^{2-}]_{-5}/[HCO_3^-]_{t_0}}, \tag{27}$$

where t_0 is the time at the onset of HCO_3^- deprotonation, $^{18}R^{t_0}_{HCO_3^-}$ is the value of $^{18}R_{HCO_3^-}$ at t_0, and $[CO_3^{2-}]_{-5}/[HCO_3^-]_{t_0}$ is the proportion of deprotonated HCO_3^-. Here we treat HCO_3^- deprotonation and $CaCO_3$ precipitation in sequence but without time-dependence (i.e. all the HCO_3^- deprotonation occurs instantaneously prior to $CaCO_3$ precipitation). Hence, $[CO_3^{2-}]_{t_1}$ in Eq. (24) is equal to $[CO_3^{2-}]_{t_0}$ plus $[CO_3^{2-}]_{-5}$ and the term $^{18}R^{t_1}_{CO_3^{2-}}$ in Eq. (25) can be expressed as the isotopic mass balance between an initial CO_3^{2-} pool prior to HCO_3^- deprotonation ($[CO_3^{2-}]_{t_0}$) and newly formed CO_3^{2-} derived from deprotonated HCO_3^- ($[CO_3^{2-}]_{-5}$):

$$^{18}R^{t_1}_{CO_3^{2-}} = \left[\left(\frac{^{18}R^{t_0}_{CO_3^{2-}}}{^{18}R^{t_0}_{CO_3^{2-}}+1}\cdot\frac{[CO_3^{2-}]_{t_0}}{[CO_3^{2-}]_{t_0}+[CO_3^{2-}]_{-5}} + \frac{R^{-5}_{CO_3^{2-}}}{R^{-5}_{CO_3^{2-}}+1}\cdot\frac{[CO_3^{2-}]_{-5}}{[CO_3^{2-}]_{t_0}+[CO_3^{2-}]_{-5}}\right)^{-1} - 1\right]^{-1}, \tag{28}$$

where $^{18}R^{t_0}_{CO_3^{2-}}$ is $^{18}R_{CO_3^{2-}}$ at t_0. Eq. (28) can be simplified because $^{18}O \ll {}^{16}O$ for all the isotopic ratios (Hayes, 1982):

$$^{18}R^{t_0}_{CO_3^{2-}} \cong \frac{^{18}R^{t_0}_{CO_3^{2-}}\cdot[CO_3^{2-}]_{t_0} + R^{-5}_{CO_3^{2-}}\cdot[CO_3^{2-}]_{-5}}{[CO_3^{2-}]_{t_0}+[CO_3^{2-}]_{-5}}. \tag{29}$$

Substituting (27) and (29) in (24) and dividing (24) by $^{18}R_w$, we obtain an expression for calculating the $\alpha_{c/w}$ of $CaCO_3$ precipitated instantaneously from a fraction of the CO_3^{2-} and HCO_3^- pools:

$$\alpha_{c/w} \cong \left(\alpha^{t_0}_{CO_3^{2-}/w}\cdot[CO_3^{2-}]_{t_0} + \alpha^{t_0}_{HCO_3^-/w}\cdot[HCO_3^-]_{t_0}\cdot\varphi_{HCO_3^-}\right)\frac{\varphi_{CO_3^{2-}}}{[CO_3^{2-}]_{+c}} \tag{30}$$

with

$$\varphi_{HCO_3^-} = 1-\left(1-[CO_3^{2-}]_{-5}/[HCO_3^-]_{t_0}\right)^{\alpha^{-5}_{CO_3^{2-}/HCO_3^-}} \tag{31}$$

and

$$\varphi_{CO_3^{2-}} = 1-\left[1-[CO_3^{2-}]_{+c}/\left([CO_3^{2-}]_{t_0}+[CO_3^{2-}]_{-5}\right)\right]^{\alpha^{+c}_{c/CO_3^{2-}}}. \tag{32}$$

Table 1
Equilibrium fractionation factors used in this study.

Equil. frac. factor	Symbol	Equation (T in Kelvin)	α at 25 °C	Reference
CO_3^{2-} – water	$\alpha^{eq}_{CO_3^{2-}/w}$	$\exp(2390\ T^{-2} - 0.00270)$	1.02448	Beck et al. (2005)
HCO_3^- – water	$\alpha^{eq}_{HCO_3^-/w}$	$\exp(2590\ T^{-2} + 0.00189)$	1.03151	Beck et al. (2005)
$CO_{2(aq)}$ – water	$\alpha^{eq}_{CO_2/w}$	$\exp(2520\ T^{-2} + 0.01212)$	1.04130	Beck et al. (2005)
CO_3^{2-} – HCO_3^-	$\alpha^{eq}_{CO_3^{2-}/HCO_3^-}$	$\alpha^{eq}_{CO_3^{2-}/w}/\alpha^{eq}_{HCO_3^-/w}$	0.99318	Calculated after Beck et al. (2005)
Calcite – CO_3^{2-}	$\alpha^{eq}_{c/CO_3^{2-}}$	Constant	1.00542	Calculated after Coplen (2007) and Beck et al. (2005)
Calcite – water	$\alpha^{eq}_{c/w}$	$\alpha^{eq}_{CO_3^{2-}/w}\cdot\alpha^{eq}_{c/CO_3^{2-}}$	1.03002	Calculated after Beck et al. (2005) and Coplen (2007)
OH^- – water	$\alpha^{eq}_{OH^-/w}$	$\exp(0.00048\ T - 0.1823)$	0.96157	Calculated after Green and Taube (1963)

The oxygen isotopic results from witherite (i.e. $BaCO_3$) precipitated quasi-instantaneously from an isotopically equilibrated DIC pool composed mainly of CO_3^{2-} and HCO_3^- (i.e. negligible $CO_{2(aq)}$; Kim et al., 2006) can be used to constrain $\alpha^{-5}_{CO_3^{2-}/HCO_3^-}$ and $\alpha^{+c}_{c/CO_3^{2-}}$ and in Eqs. (31) and (32). For $\alpha^{+c}_{c/CO_3^{2-}}$, we assume that the ^{18}O-^{16}O difference in reaction rates during calcite precipitation are similar to that of witherite precipitation. Kim et al. (2006) found that the oxygen isotope fractionation between $BaCO_3$ and H_2O ($\alpha_{Ba/w}$) increased with increasing fractions of the CO_3^{2-} pool consumed as well as with increasing fraction of deprotonated HCO_3^-, suggesting that isotopically light CO_3^{2-} ions are preferentially incorporated into $BaCO_3$ and isotopically light HCO_3^- ions are preferentially deprotonated (Kim et al., 2006; Fig. 4A). We estimated the KIFF $\alpha^{-5}_{CO_3^{2-}/HCO_3^-}$ and $\alpha^{+c}_{c/CO_3^{2-}}$ at 25 °C by fitting Eq. (30) to the data of Kim et al. (2006) using the following known values and relationships (Fig. 4A):

i. $\alpha^{t_0}_{CO_3^{2-}/w}$ and $\alpha^{t_0}_{HCO_3^-/w}$ are given by the equilibrium fractionation factors $\alpha^{eq}_{CO_3^{2-}/w}$ (1.0240) and $\alpha^{eq}_{HCO_3^-/w}$ (1.0310) at 25 °C (as in Kim et al., 2006).
ii. $[CO_3^{2-}]_{t_0}$ and $[HCO_3^-]_{t_0}$ are obtained from the solution pH and ionic content prior to the addition of NaOH (as in Kim et al., 2006).
iii. $[CO_3^{2-}]_{+c}$ is obtained from the molar concentration of DIC consumed (as in Kim et al., 2006).
iv. $[CO_3^{2-}]_{-5} = 0$ where $[CO_3^{2-}]_{+c} < [CO_3^{2-}]_{t_0}$ and $[CO_3^{2-}]_{-5} = [CO_3^{2-}]_{+c} - [CO_3^{2-}]_{t_0}$ where $[CO_3^{2-}]_{+c} > [CO_3^{2-}]_{t_0}$ (these relations assume that all of the deprotonated HCO_3^- ions precipitate as $BaCO_3$).

Given the constraints listed above, the best agreement between model and data is obtained with $\alpha^{+c}_{c/CO_3^{2-}} = 0.9995 \pm 0.0002$ and $\alpha^{-5}_{CO_3^{2-}/HCO_3^-} = 0.9950 \pm 0.0002$ (Fig. 4A and B, $r^2 = 0.98$, p-value < 0.01; Table 2). Our estimate of the $CaCO_3$-CO_3^{2-} KIFF ($\alpha^{+c}_{c/CO_3^{2-}}$) is closer to unity than that of Watkins et al. (2014) ($\alpha^{+c}_{c/CO_3^{2-}} = 0.9980$). The latter was deduced from an isotopic ion-by-ion growth model (Wolthers et al., 2012) and $\alpha_{c/w}$ versus growth rate data (Watkins et al., 2014). These authors estimated $\alpha^{+c}_{c/CO_3^{2-}}$ using a $\alpha^{eq}_{CO_3^{2-}/w}$ value of 1.0268 (at 25 °C), based on the equation of Wang et al. (2013). Adjusting the result of Watkins et al. (2014) for a preferred $\alpha^{eq}_{CO_3^{2-}/w}$ value within 1.0240 and 1.0245 (Beck et al., 2005; Kim et al., 2006, 2014), yields $\alpha^{+c}_{c/CO_3^{2-}} = 1.0003$–$1.0008$, which is above unity and inconsistent with a preferential precipitation of isotopically light CO_3^{2-} ions. In short, these results suggest that the transfer of carbonate ions from the solution to the carbonate mineral induces a small oxygen isotopic fractionation of −0.5‰ at the kinetic limit. In contrast to the small KIFF during CO_3^{2-} transfer to $CaCO_3$, the KIFF during HCO_3^- deprotonation ($\alpha^{-5}_{CO_3^{2-}/HCO_3^-}$) results in newly formed CO_3^{2-} with an $^{18}O/^{16}O$ ~5‰ lower than the parent HCO_3^-.

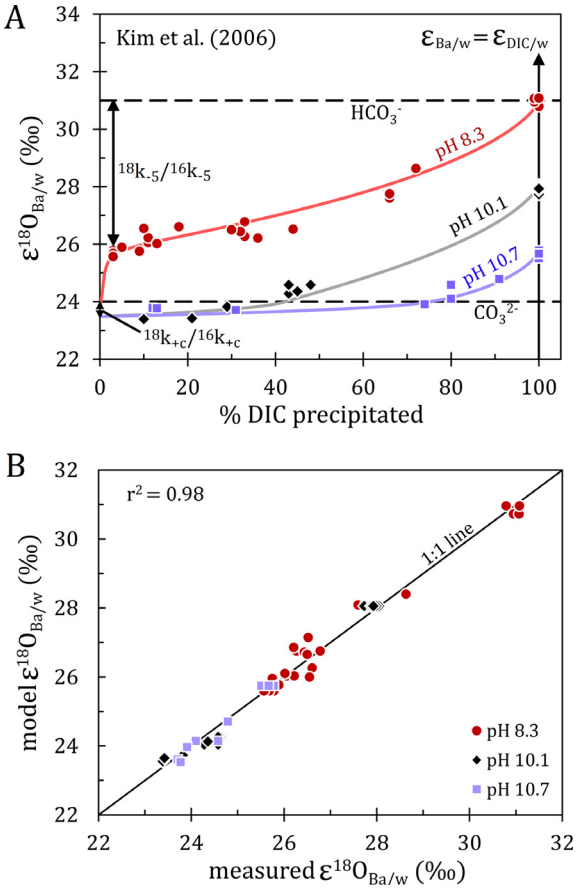

Fig. 4. The effect of pH and partial DIC precipitation on the oxygen isotope fractionation between instantaneously precipitated $BaCO_3$ and water ($\varepsilon_{Ba/w}$) at 25 °C (data from Kim et al., 2006). (A) Comparison of measured and modelled $\varepsilon_{Ba/w}$ at pH 8.3, 10.1 and 10.7, as a function of the proportion of DIC precipitated. (B) Measured versus modelled $\varepsilon_{Ba/w}$ values ($r^2 = 0.98$, p-value < 0.01). These diagrams show the best agreement between measured and modelled $\varepsilon_{Ba/w}$ obtained with a KIFF between the carbonate mineral and CO_3^{2-} ($^{18}k_{+c}/^{16}k_{+c}$) of 0.9995 and a CO_3^{2-}-HCO_3^- KIFF ($^{18}k_{-5}/^{16}k_{-5}$, HCO_3^- deprotonation) of 0.9950. The preferential precipitation of isotopically light CO_3^{2-} ions and the preferential deprotonation of isotopically light HCO_3^- make $BaCO_3$ depleted in ^{18}O relative to the DIC pool where precipitation is instantaneous but not quantitative.

4.3. Isotopic fractionation between DIC species and water ($\alpha_{CO_3^{2-}/w}$ and $\alpha_{HCO_3^-/w}$)

4.3.1. Kinetic vs equilibrium fractionation

An equilibrium distribution of DIC species in solution is achieved within seconds, but oxygen isotopic equilibration takes hours or days depending on the solution pH and temperature (McConnaughey, 1989b; Usdowski et al., 1991; Zeebe and Wolf-Gladrow, 2001; Beck et al., 2005). The relatively slow isotopic exchange between DIC species and

Table 2
Kinetic isotope fractionation factors used in this study.

Kinetic isotope fractionation[a]	Symbol	Value at 25 °C	Note
$CaCO_3$ – CO_3^{2-}	$^{18}k_{+c}/^{16}k_{+c}$	0.9995 ± 0.0002	Calculated after Kim et al. (2006)
CO_3^{2-} – HCO_3^-	$^{18}k_{-5}/^{16}k_{-5}$	0.9950 ± 0.0002	Calculated after Kim et al. (2006)
HCO_3^- – (CO_2+H_2O)	$^{18}k_{+2}/^{16}k_{+2}$	0.9994 ± 0.0010	Calculated after Zeebe (2014)
HCO_3^- – (CO_2+OH^-)	$^{18}k_{+4}/^{16}k_{+4}$	0.9958 ± 0.0003	Model parameter

[a] For example, a $^{18}k_{+c}/^{16}k_{+c}$ of 0.9995 ± 0.0002 at 25 °C indicates that the product ($CaCO_3$) has a lower $^{18}O/^{16}O$ than the reactant (CO_3^{2-}).

water occurs via the hydration and hydroxylation reactions (McConnaughey, 1989b; Usdowski et al., 1991):

$$CO_2 + H_2O \overset{k^*_{-2},\ k^*_{+2}}{\Longleftrightarrow} H_2CO_3 \Longleftrightarrow HCO_3^- + H^+ \quad \text{(hydration)} \tag{33}$$

and

$$CO_2 + OH^- \overset{k_{-4},\ k_{+4}}{\Longleftrightarrow} HCO_3^- \quad \text{(hydroxylation)}, \tag{34}$$

where k^*_{-2}, k^*_{+2} and k_{-4}, k_{+4} are the backward and forward reaction rate constants for CO_2 hydration and hydroxylation, respectively (the superscript * of k^*_{-2} and k^*_{+2} denote the inclusion of the effect of carbonic anhydrase on the rate of CO_2 (de)hydration; see Appendix A.4 for calculation of rate constants). Usdowski et al. (1991) derived an expression for the oxygen isotope ratio of the DIC as a function of time:

$$ln\left(\frac{^{18}R^t_{DIC} - {}^{18}R^{eq}_{DIC}}{^{18}R^{t_0}_{DIC} - {}^{18}R^{eq}_{DIC}}\right) = \frac{-t}{\tau}, \tag{35}$$

where t is the time spent by the DIC pool in solution, τ is the time constant and $^{18}R^t_{DIC}$, $^{18}R^{t_0}_{DIC}$ and $^{18}R^{eq}_{DIC}$ are the oxygen isotope ratios of DIC at time t, t_0 and at isotopic equilibrium. Eq. (35) can be rewritten to express the oxygen isotope ratio of DIC at time t:

$$^{18}R^t_{DIC} = e^{\left(\frac{-t}{\tau}\right)}\left(^{18}R^{t_0}_{DIC} - {}^{18}R^{eq}_{DIC}\right) + {}^{18}R^{eq}_{DIC}. \tag{36}$$

Dividing Eq. (36) by $^{18}R_w$ provides an equation for the oxygen isotope fractionation between the DIC pool and water:

$$\alpha^t_{DIC/w} = e^{\left(\frac{-t}{\tau}\right)}\left(\alpha^{t_0}_{DIC/w} - \alpha^{eq}_{DIC/w}\right) + \alpha^{eq}_{DIC/w}. \tag{37}$$

The rate of protonation and deprotonation among H_2CO_3, HCO_3^- and CO_3^{2-} ions is several orders of magnitude faster than the CO_2 hydration and hydroxylation reactions (Zeebe and Wolf-Gladrow, 2001). Therefore, where gaseous CO_2 is the dominant DIC source for $CaCO_3$ precipitation and the system is at steady state, it can be assumed that H_2CO_3, HCO_3^- and CO_3^{2-} remain at isotopic equilibrium with each other (but not with H_2O) over the course of DIC-H_2O isotopic equilibration (this is in contrast with a unidirectional deprotonation of HCO_3^- during instantaneous carbonate precipitation; Section 4.2.4). Consequently, Eq. (37) can be rewritten for any of the DIC species (i):

$$\alpha^t_{i/w} = e^{\left(\frac{-t}{\tau}\right)}\left(\alpha^{t_0}_{i/w} - \alpha^{eq}_{i/w}\right) + \alpha^{eq}_{i/w}. \tag{38}$$

Note that where $\tau << t$, $\alpha^t_{i/w} = \alpha^{eq}_{i/w}$ (i.e. the equilibrium isotopic ratio of the DIC species). The level of isotopic equilibrium between DIC species and water (E_{DIC}) can therefore be expressed as:

$$E_{DIC} = 1 - e^{\left(\frac{-t}{\tau}\right)}. \tag{39}$$

The time constant τ in Eqs. (38) and (39) is a function of the hydration and hydroxylation reaction kinetics (Usdowski et al., 1991; Uchikawa and Zeebe, 2012; Appendix A.5), which in turn depends on DIC speciation (Millero et al., 2006; Appendix A.6), pH and temperature. Solving Eq. (38) requires knowledge of the residence time of the DIC in solution (RT_{DIC}). Under steady state conditions, RT_{DIC} is equal to the molar quantity of DIC divided by the calcite growth rate in moles/s:

$$RT_{DIC} = \frac{[DIC]V}{r_c}, \tag{40}$$

where V is the volume of the precipitating solution. The following sections present equations for the equilibrium ($\alpha^{eq}_{i/w}$) and kinetic ($\alpha^{t_0}_{i/w}$) end members of Eq. (38).

4.3.2. Equilibrium fractionations between DIC species and water

The oxygen isotope fractionations between the DIC species and water under equilibrium conditions were determined by Beck et al. (2005) over the 15–40 °C temperature range and by Kim and co-workers at 25 °C and over varying ionic strength (Kim et al., 2006, 2014). These studies showed that the relationships determined by Beck et al. (2005) can be applied to solutions of different solute content and ionic strength (Table 1). Alternative fractionation factors were also derived by Wang et al. (2013) based on the experimental data of Beck et al. (2005) and Kim et al. (2006). Recent work by Kim et al. (2014) confirmed the initial results of Beck et al. (2005), and hence the equations from Beck et al. (2005) were used in this study (Table 1).

4.3.3. Kinetic isotope fractionation during the hydration and hydroxylation of CO_2

When gaseous CO_2 dissolves in water with a pH higher than 7, most of the CO_2 is rapidly converted into HCO_3^- and CO_3^{2-} ions via the hydration and/or hydroxylation reaction pathways (Section 4.3.1). The initial oxygen isotope ratios of 'HCO_3^- plus CO_3^{2-}' ($^{18}R^{t_0}_{(CO_3^{2-}+HCO_3^-)}$) reflects

the oxygen atoms from the molecules or ions involved in the CO_2 hydration and/or hydroxylation reactions. The parameter $\alpha^{t_0}_{(CO_3^{2-}+HCO_3^-)/w}$ is defined as the initial (kinetic) oxygen isotope fractionation between hydrated/hydroxylated CO_2 and water:

$$\alpha^{t_0}_{(CO_3^{2-}+HCO_3^-)/w} = \frac{{}^{18}R^{t_0}_{(CO_3^{2-}+HCO_3^-)}}{{}^{18}R_w}. \quad (41)$$

In turn, ${}^{18}R^{t_0}_{(CO_3^{2-}+HCO_3^-)}$ is equal to the isotopic mass-balance between the initial oxygen isotopic ratios of hydrated and hydroxylated CO_2:

$${}^{18}R^{t_0}_{(CO_3^{2-}+HCO_3^-)} \cong {}^{18}R^{+2}_{(CO_3^{2-}+HCO_3^-)} \cdot X_{+2} + {}^{18}R^{+4}_{(CO_3^{2-}+HCO_3^-)} \cdot X_{+4}, \quad (42)$$

where ${}^{18}R^{+2}_{(CO_3^{2-}+HCO_3^-)}$ and ${}^{18}R^{+4}_{(CO_3^{2-}+HCO_3^-)}$ are the initial oxygen isotopic ratios of hydrated and hydroxylated CO_2, respectively, and where X_{+2} and X_{+4} are the relative proportions of hydrated and hydroxylated CO_2, respectively. The relative importance of CO_2 hydration versus CO_2 hydroxylation depends on solution pH (Johnson, 1982). According to reactions pathways (33) and (34), X_{+2} and X_{+4} are expressed as follows:

$$X_{+2} = \frac{k^*_{+2}}{k^*_{+2} + k_{+4}[OH^-]} \quad (43)$$

and

$$X_{+4} = \frac{k_{+4}[OH^-]}{k^*_{+2} + k_{+4}[OH^-]}. \quad (44)$$

The concentration of hydroxyl ions $[OH^-]$ in Eqs. (43) and (44) is obtained from the stoichiometric ion product of water K^*_w (DOE, 1994; Appendix A.7) and pH. Solving (42) requires knowledge of ${}^{18}R^{+2}_{(CO_3^{2-}+HCO_3^-)}$ and ${}^{18}R^{+4}_{(CO_3^{2-}+HCO_3^-)}$. For the hydration reaction, ${}^{18}k_{+2}$ and ${}^{16}k_{+2}$ are defined as rate coefficients of ^{16}O and ^{18}O transfer between the sum of the reactants '$CO_{2(aq)}$ and H_2O' and hydrated CO_2 (i.e. mainly the sum of HCO_3^- and CO_3^{2-}). Where the reaction is strictly forward the ${}^{18}k_{+2}/{}^{16}k_{+2}$ ratio is related to the oxygen isotopic ratios of reactants ($CO_{2(aq)} + H_2O$) and products (HCO_3^- and CO_3^{2-}):

$$\frac{{}^{18}k_{+2}}{{}^{16}k_{+2}} = \frac{{}^{18}R^{+2}_{(CO_3^{2-}+HCO_3^-)}}{{}^{18}R_{(CO_2+w)}}, \quad (45)$$

where ${}^{18}R_{(CO_2+w)}$ is the oxygen isotopic ratio of '$CO_{2(aq)} + H_2O$'. Rearranging (45) provides an equation for ${}^{18}R^{+2}_{(CO_3^{2-}+HCO_3^-)}$ as a function of the ${}^{18}k_{+2}/{}^{16}k_{+2}$ ratio:

$${}^{18}R^{+2}_{(CO_3^{2-}+HCO_3^-)} = {}^{18}R_{(CO_2+w)} \cdot \frac{{}^{18}k_{+2}}{{}^{16}k_{+2}}. \quad (46)$$

With a contribution of two oxygen atoms from $CO_{2(aq)}$ and one from H_2O, ${}^{18}R_{(CO_2+w)}$ is expressed as:

$${}^{18}R_{(CO_2+w)} \cong {}^{18}R_{CO_2} \cdot \frac{2}{3} + {}^{18}R_w \cdot \frac{1}{3}. \quad (47)$$

The value of ${}^{18}k_{+2}/{}^{16}k_{+2}$ in Eq. (45) has yet to be determined experimentally but theoretical calculations based on transition state theory and quantum chemistry suggest an overall kinetic fractionation factor between hydrated CO_2 and $CO_{2(aq)}$ ($\alpha^{+2}_{(CO_3^{2-}+HCO_3^-)/CO_2}$) of 0.986 ± 0.001 (Zeebe, 2014). Note that Zeebe (2014) presented results for the kinetic fractionation factor between $CO_{2(aq)}$ and hydrated CO_2 (1.014 ± 0.001), and thus the fractionation factor between hydrated CO_2 and $CO_{2(aq)}$ is the inverse of 1.014. The initial oxygen isotope ratio of hydrated CO_2 can therefore be expressed as a function of $\alpha^{+2}_{(CO_3^{2-}+HCO_3^-)/CO_2}$:

$${}^{18}R^{+2}_{(CO_3^{2-}+HCO_3^-)} = {}^{18}R_{CO_2} \cdot \alpha^{+2}_{(CO_3^{2-}+HCO_3^-)/CO_2}, \quad (48)$$

where ${}^{18}R_{CO_2}$ is the oxygen isotope ratio of $CO_{2(aq)}$. Substituting (48) and (47) into (46) yields an equation for ${}^{18}k_{+2}/{}^{16}k_{+2}$ as a function of $\alpha^{+2}_{(CO_3^{2-}+HCO_3^-)/CO_2}$:

$$\frac{{}^{18}k_{+2}}{{}^{16}k_{+2}} = \frac{\alpha^{+2}_{(CO_3^{2-}+HCO_3^-)/CO_2}}{2/3 + 1/3 \cdot (\alpha_{CO_2/w})^{-1}}. \quad (49)$$

Using the equilibrium value of Beck et al. (2005) for $\alpha_{CO_2/w}$ (Table 1) and a value of 0.986 ± 0.001 for $\alpha^{+2}_{(CO_3^{2-}+HCO_3^-)/CO_2}$ (Zeebe, 2014) yields a ${}^{18}k_{+2}/{}^{16}k_{+2}$ ratio of 0.9994 ± 0.0010 at 25 °C. This calculation suggests that the mass-related KIE during CO_2 hydration is on the order of 1‰ or less. The 14‰ depletion in ^{18}O between hydrated CO_2 and $CO_{2(aq)}$ ($\alpha^{+2}_{(CO_3^{2-}+HCO_3^-)/CO_2} = 0.986 \pm 0.001$, Zeebe, 2014) is therefore mainly caused by the contribution of oxygen atoms from CO_2 and H_2O.

Similar to the hydration reaction above, we define ${}^{18}k_{+4}$ and ${}^{16}k_{+4}$ as rate coefficients of ^{16}O and ^{18}O transfer between hydroxylated CO_2 (i.e. mainly the sum of HCO_3^- and CO_3^{2-}) and the sum of the reactant $CO_{2(aq)}$ and OH^-:

$$\frac{{}^{18}k_{+4}}{{}^{16}k_{+4}} = \frac{{}^{18}R^{+4}_{(CO_3^{2-}+HCO_3^-)}}{{}^{18}R_{(CO_2+OH^-)}}, \quad (50)$$

where ${}^{18}R_{(CO_2+OH^-)}$ is the oxygen isotopic ratio of '$CO_{2(aq)} + OH^-$'. Rearranging Eq. (50), we have:

$${}^{18}R^{+4}_{(CO_3^{2-}+HCO_3^-)} = {}^{18}R_{(CO_2+OH^-)} \cdot \frac{{}^{18}k_{+4}}{{}^{16}k_{+4}}. \quad (51)$$

With a contribution of two oxygen atoms from $CO_{2(aq)}$ and one from OH^-, ${}^{18}R_{(CO_2+OH^-)}$ is expressed as:

$${}^{18}R_{(CO_2+OH^-)} \cong {}^{18}R_{CO_2} \cdot \frac{2}{3} + {}^{18}R_{OH^-} \cdot \frac{1}{3}, \quad (52)$$

where ${}^{18}R_{OH^-}$ is the oxygen isotope ratio of OH^- ions. The temperature dependence of the equilibrium oxygen isotope fractionation between OH^- and H_2O ($\alpha^{eq}_{OH^-/w}$) was estimated by Green and Taube (1963) (Table 1). The ${}^{18}k_{+4}/{}^{16}k_{+4}$ ratio has not been accurately measured or estimated yet, and is thus treated as a free parameter of the model.

The equations presented thus far allow for calculation of the initial oxygen isotope ratio of the sum of CO_3^{2-} and HCO_3^- but not of CO_3^{2-} or HCO_3^- individually. The parameter ${}^{18}R^{t_0}_{CO_3^{2-}+HCO_3^-}$ in Eq. (42) can be expressed as the isotopic

mass balance between the initial oxygen isotope ratio of CO_3^{2-} ($^{18}R^{t_0}_{CO_3^{2-}}$) and HCO_3^- ($^{18}R^{t_0}_{HCO_3^-}$):

$$^{18}R^{t_0}_{(CO_3^{2-}+HCO_3^-)} \cong {}^{18}R^{t_0}_{CO_3^{2-}} \cdot X_{CO_3^{2-}} + {}^{18}R^{t_0}_{HCO_3^-} \cdot X_{HCO_3^-}, \quad (53)$$

where $X_{CO_3^{2-}}$ and $X_{HCO_3^-}$ are the relative proportions of CO_3^{2-} and HCO_3^- ions, respectively, and are obtained from the first and second dissociation constants of carbonic acid (Millero et al., 2006; Appendix A.6). As mentioned in Section 4.3.1, CO_3^{2-} and HCO_3^- are considered to be in isotopic equilibrium with each other due to the fast rate of protonation and deprotonation between these species relative to the rate of the hydration and hydroxylation reactions. The ratio of $^{18}R^{t_0}_{CO_3^{2-}}$ to $^{18}R^{t_0}_{HCO_3^-}$ is therefore equal to the equilibrium fractionation factor between CO_3^{2-} and HCO_3^- ($\alpha^{eq}_{CO_3^{2-}/HCO_3^-}$):

$$\frac{^{18}R^{t_0}_{CO_3^{2-}}}{^{18}R^{t_0}_{HCO_3^-}} = \alpha^{eq}_{CO_3^{2-}/HCO_3^-}. \quad (54)$$

Substituting (54) into (53) and dividing each isotopic ratio by $^{18}R_w$, expressions for $\alpha^{t_0}_{CO_3^{2-}/w}$ and $\alpha^{t_0}_{HCO_3^-/w}$ are as follows:

$$\alpha^{t_0}_{CO_3^{2-}/w} \cong \frac{\alpha^{t_0}_{(CO_3^{2-}+HCO_3^-)/w}}{X_{CO_3^{2-}} + X_{HCO_3^-} \cdot \left(\alpha^{eq}_{CO_3^{2-}/HCO_3^-}\right)^{-1}} \quad (55)$$

and

$$\alpha^{t_0}_{HCO_3^-/w} \cong \frac{\alpha^{t_0}_{(CO_3^{2-}+HCO_3^-)/w}}{X_{CO_3^{2-}} \cdot \alpha^{eq}_{CO_3^{2-}/HCO_3^-} + X_{HCO_3^-}}. \quad (56)$$

The value of $\alpha^{eq}_{CO_3^{2-}/HCO_3^-}$ in Eqs. (55) and (56) is obtained from the equilibrium isotopic fractionation factors $\alpha^{eq}_{CO_3^{2-}/w}$ and $\alpha^{eq}_{HCO_3^-/w}$ (Beck et al., 2005; Table 1):

$$\alpha^{eq}_{CO_3^{2-}/HCO_3^-} = \frac{\alpha^{eq}_{CO_3^{2-}/w}}{\alpha^{eq}_{HCO_3^-/w}}. \quad (57)$$

From this set of equations it is possible to calculate, and display graphically, the kinetic limits $\alpha^{t_0}_{CO_3^{2-}/w}$ and $\alpha^{t_0}_{HCO_3^-/w}$ as a function of temperature and chemical speciation (Fig. 5). The increasing contribution of the hydroxylation reaction and increasing CO_3^{2-}/HCO_3^- ratio with increasing pH (Fig. 5A) make $\alpha^{t_0}_{CO_3^{2-}/w}$ and $\alpha^{t_0}_{HCO_3^-/w}$ highly sensitive to changes in solution pH (Fig. 5B). Overall, both $\alpha^{t_0}_{CO_3^{2-}/w}$ and $\alpha^{t_0}_{HCO_3^-/w}$ decrease with increasing pH, although minimum values are attained when the hydroxylation/hydration reaction rate ratio is near the maximum value but the CO_3^{2-}/HCO_3^- ratio is low (vertical line in Fig. 5A and B). For a solution at 25 °C and salinity of 2–3 g/kg, both $\alpha^{t_0}_{CO_3^{2-}/w}$ and $\alpha^{t_0}_{HCO_3^-/w}$ reach minimum values at pH ~ 9.6 (Fig. 5B). Since in our model CO_3^{2-} is the only precipitating DIC species, the kinetic limit of $\alpha_{c/w}$ is always ~ 0.5‰ lower than $\alpha^{t_0}_{CO_3^{2-}/w}$ (see Section 4.2.4). At high pH, the $\alpha^{t_0}_{CO_3^{2-}/w}$ and $\alpha^{t_0}_{HCO_3^-/w}$ values and the kinetic limit of $\alpha_{c/w}$ depend on the $^{18}k_{+4}/^{16}k_{+4}$ ratio, which is constrained by experimental data in Section 5.3.

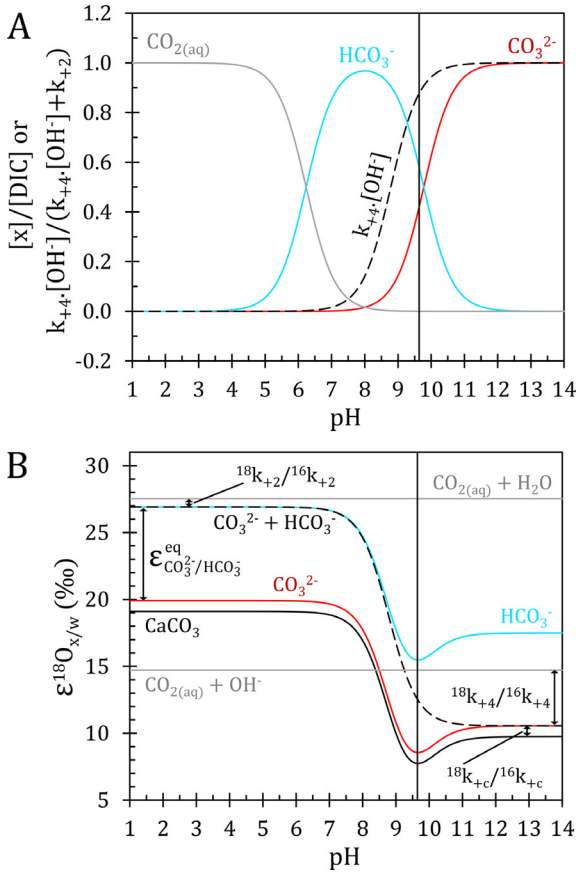

Fig. 5. Kinetic isotope fractionation in the $CaCO_3$-DIC-H_2O system during the hydration and hydroxylation of CO_2. (A) DIC speciation (solid lines) and relative importance of the hydroxylation vs hydration reaction (dash line) as a function of pH for T = 25 °C and $I = 0.05$. (B) Initial oxygen isotope fractionation (kinetic limit) relative to water for CO_3^{2-}, HCO_3^- and $CaCO_3$ following the hydration and hydroxylation of CO_2 in the solution defined in (A). In (B), the CO_3^{2-} (red) and HCO_3^- (light blue) lines were constructed with an equilibrium fractionation factor between CO_3^{2-} and HCO_3^- ($\varepsilon^{eq}_{CO_3^{2-}/HCO_3^-}$) of 0.9932 and a pH-dependent fractionation factor between hydrated/hydroxylated CO_2 (i.e., $CO_3^{2-} + HCO_3^-$, dashed line) and water varying from 1.0269 to 1.0105. For the CO_2 hydration reaction, the mass dependent kinetic isotope fractionation ($^{18}k_{+2}/^{16}k_{+2} = 0.9994$) is seen in the difference between the "$CO_3^{2-} + HCO_3^-$" and "$CO_{2(aq)} + H_2O$" lines at low pH values. For the CO_2 hydroxylation reaction, the mass dependent kinetic fractionation ($^{18}k_{+4}/^{18}k_{+4} = 0.9958$) is seen in the difference between the "$CO_3^{2-} + HCO_3^-$" and "$CO_{2(aq)} + OH^-$" lines at high pH values. Instantaneously precipitated $CaCO_3$ from a small fraction of the CO_3^{2-} pool would be depleted by ~ 0.5‰ ($^{18}k_{+c}/^{16}k_{+c} = 0.9995$) relative to the CO_3^{2-} pool (black continuous line). The fractionations relative to water for CO_3^{2-}, HCO_3^- and $CaCO_3$ are lowest where the hydroxylation/hydration reaction rate ratio is high but the CO_3^{2-}/HCO_3^- ratio is low (vertical line in panel A and B). For a CO_2-fed solution at 25 °C, the kinetic limit of the oxygen isotope fractionation between $CaCO_3$ and water depends on the solution pH and varies from 19.5 to 8.5‰ (i.e. 1.0195–1.0085) between pH 7 and 9.6.

5. DATA-MODEL COMPARISON

5.1. Experimental data

We used the temperatures, pH, salinities, [DIC], [Ca^{2+}], calcite growth rates and carbonic anhydrase activities from the calcite growth experiments of Dietzel et al. (2009) and Baker (2015) to calculate model calcite-H_2O fractionation factors for comparison to measured calcite-H_2O fractionation factors. In both Dietzel and Baker experiments, the source of DIC was gaseous CO_2 and the solution pH was maintained constant while calcite was precipitated at various temperature, pH and Ω. In the experiments of Dietzel et al. (2009), $CO_{2(g)}$ diffused passively across a membrane from an inner solution to the precipitating solution. In the experiments of Baker (2015), $CO_{2(g)}$ was bubbled directly into the precipitating solution. The $\delta^{18}O$ of the incoming $CO_{2(g)}$ ranged from 28.6 to 30.1‰ (VSMOW) for the experiments of Baker (2015) but it was not reported by Dietzel et al. (2009). However, for the experiments of Dietzel et al. (2009), we assumed that $CO_{2(aq)}$ entered the precipitating solution at isotopic equilibrium with water since the $CO_{2(g)}$ originated from an external solution rather than a gas tank.

Monitoring of the DIC concentration during the experiments of Baker (2015) suggests (near) steady state conditions during calcite precipitation. In the experiments of Dietzel et al. (2009), the DIC concentration was only measured at the onset of calcite precipitation. For our data-model comparison, we assumed that in each of Dietzel's experiments, calcite precipitated under steady state conditions and the DIC concentration decreased in a similar manner as in the experiments of Baker (2015). We therefore base our calculations on an average [DIC] concentration of $2/3 \pm 1/3$ of the initial [DIC] reported by Dietzel et al. (2009) (i.e. 33–100% of the reported maximum [DIC]).

Calculated isotopic equilibration levels between DIC and water (E_{DIC}; Eq. (39), Table 3 and Fig. 6A) indicate that calcite was precipitated from an isotopically equilibrated DIC pool ($E_{DIC} > 0.99$) in all of Baker's experiments (due to the presence of the enzyme carbonic anhydrase in solution), and in at least 15 of the 40 experiments conducted by Dietzel et al. (2009). The remaining 25 experiments of Dietzel et al. (2009) display a wide range of E_{DIC} values from 0.01 to 0.99. The range of calculated E_{DIC} is due to the differences in pH, [DIC] and calcite growth rate among the experiments (Table 3). A plot of $\alpha_{c/w}$ versus temperature (Fig. 6B) for the experimental data of Dietzel et al. (2009) and Baker (2015) confirms that most of the scatter in $\alpha_{c/w}$ values reported by Dietzel et al. (2009) arises from non-equilibrated DIC pool ($E_{DIC} \leq 0.99$). On the other hand, the data of Dietzel et al. (2009) and Baker (2015) are in good agreement when considering $\alpha_{c/w}$ from experiments with $E_{DIC} > 0.99$ (Fig. 6B). Importantly, the average temperature sensitivity of $\alpha_{c/w}$ between 5 and 40 °C obtained using Dietzel's and Baker's data with $E_{DIC} > 0.99$ is equal to -0.21 ± 0.01‰/°C, which is within error of the temperature sensitivity of $\alpha_{CO_3^{2-}/w}$ (-0.19 ± 0.01‰/°C, Beck et al., 2005) and very similar to the temperature sensitivity reported by Kim and O'Neil (1997) for $\alpha_{c/w}$ (-0.22‰/°C).

In the following sections, the equilibrium $\alpha_{CO_3^{2-}/w}$ values (Beck et al., 2005) and the measured $\alpha_{c/w}$ values of Dietzel and Baker for the experiments where $E_{DIC} > 0.99$ are used to infer $\alpha_{c/CO_3^{2-}}$ values for those experiments, and to fine-tune the model parameter n_2. The quantification of these parameters then allows us to investigate and quantify KIE between CO_3^{2-} and H_2O for experiments where $E_{DIC} \leq 0.99$.

5.2. Calcite precipitated from isotopically equilibrated DIC

Where calcite precipitates from an isotopically equilibrated DIC pool, $\alpha_{c/w}$ is independent of the DIC source(s) because H_2O is by far the dominant oxygen-bearing species and the $^{18}O/^{16}O$ of the DIC species reflect the known fractionations between DIC species and water (Table 1, Beck et al., 2005). Thus, the only model unknown is the fractionation between calcite and CO_3^{2-} ($\alpha_{c/CO_3^{2-}}$), which can be inferred from a measured $\alpha_{c/w}$ value and the known $\alpha^{eq}_{CO_3^{2-}/w}$ value (see Eq. (6)). Calculated $\alpha_{c/CO_3^{2-}}$ values for experimental conditions where $E_{DIC} > 0.99$ vary from 1.0028 to 1.0049 (Fig. 7A, 'measured' $\varepsilon_{c/CO_3^{2-}}$) and appear independent of temperature and experimental setup. Importantly, the $\alpha_{c/CO_3^{2-}}$ values are negatively correlated with the calcite saturation state ($r^2 = 0.34$, p-value $= 0.003$) and are closer to the equilibrium limit ($\alpha^{eq}_{c/CO_3^{2-}} = 1.0054$) than the kinetic limit ($\alpha^{+c}_{c/CO_3^{2-}} = 0.9995$). The lack of a significant temperature effect on $\alpha_{c/CO_3^{2-}}$ (Fig. 7A) implies that the $\alpha^{eq}_{c/CO_3^{2-}}$ and $\alpha^{+c}_{c/CO_3^{2-}}$ limits are also independent of temperature and can thus be considered as constants. This is an important finding as it implies that the temperature sensitivity of calcite $^{18}O/^{16}O$ originates from the effect of temperature on the $^{18}O/^{16}O$ of CO_3^{2-}. Using the known temperature sensitivity of $\alpha^{eq}_{CO_3^{2-}/w}$ and constant values for $\alpha^{eq}_{c/CO_3^{2-}}$ and $\alpha^{+c}_{c/CO_3^{2-}}$ (Tables 1 and 2), the $\alpha^{eq}_{c/w}$ and $\alpha^{+c}_{c/w}$ can be expressed as a function of temperature (T in Kelvin):

$$\alpha^{eq}_{c/w} = \exp(2390T^{-2} - 0.0027) \cdot 1.00542 \quad (56)$$

and

$$\alpha^{+c}_{c/w} = \exp(2390T^{-2} - 0.0027) \cdot 0.9995. \quad (57)$$

In the model, $\alpha_{c/w}$ varies between $\alpha^{eq}_{c/w}$ and $\alpha^{+c}_{c/w}$ as a function of Ω and the partial reaction order n_2 (Fig. 3, Section 4.2.2). The parameter n_2 could not be derived directly from the available data but is estimated using a sensitivity analysis of model-data agreement for n_2 values varying from 0.1 to 1.0 (Fig. 7B). Measured and modelled $\alpha_{c/w}$ values agree best at $n_2 = 0.22 \pm 0.02$ (Fig. 7B and C, average $|\Delta^{18}O_{data-model}| = 0.25$‰, $r^2 = 0.96$, p-value < 0.001) for both experimental studies and for all

Table 3
Model input and output parameters for the calcite growth experiment of Dietzel et al. (2009) and Baker (2015).

ID[a]	T (°C)	pH_{NBS}	[DIC][b] μmol/kg	σ	[Ca^{2+}] μmol/kg	r_c nmol/s/L	[CA] μmol/kg	Ω[c]	E_{DIC}[c]	E_c[c,d]	Measured $\varepsilon^{18}O$ (‰)	σ	Modelled $\varepsilon^{18}O$ (‰)[c,d]	pos σ	neg σ
B14	25	7.50	1085	109	15,000	55.04	0.23	3.24	1.00	0.78	28.78	0.12	28.78	0.17	0.13
B15	25	7.50	1100	110	15,000	21.35	0.24	3.28	1.00	0.78	28.64	0.12	28.77	0.17	0.13
B3	25	8.30	222	22	15,000	11.82	0.23	4.25	1.00	0.74	28.39	0.12	28.50	0.16	0.12
B4	25	8.30	217	22	15,000	8.02	0.34	4.15	1.00	0.74	28.38	0.12	28.52	0.16	0.12
B7	25	8.65	141	28	15,000	13.05	0.34	5.84	1.00	0.69	28.30	0.12	28.19	0.24	0.17
B8	25	8.65	139	28	15,000	14.17	0.22	5.75	1.00	0.69	28.38	0.12	28.21	0.24	0.17
B5	25	9.00	140	28	15,000	20.35	0.35	11.97	1.00	0.59	28.22	0.12	27.57	0.21	0.15
B12	25	9.30	60	18	15,000	15.30	0.55	8.96	1.00	0.63	28.07	0.12	27.81	0.33	0.22
D1	5	9.00	160	80	9520	0.50	0.00	6.49	1.00	0.68	27.11	0.15	32.33	0.37	1.14
D2	5	9.00	160	80	9380	0.72	0.00	6.43	0.99	0.68	28.63	0.15	32.21	0.33	2.66
D3	5	9.00	220	110	9540	2.40	0.00	8.91	0.85	0.63	29.93	0.15	29.68	2.61	6.40
D4	5	10.00	33	17	9210	1.24	0.00	7.13	0.17	0.66	14.19	0.15	15.21	3.74	2.63
D5	5	8.50	353	177	9830	0.61	0.00	4.95	1.00	0.71	32.01	0.15	32.63	0.41	0.85
D6	5	10.50	27	14	91,260	3.68	0.00	14.47	0.01	0.57	13.16	0.15	13.15	0.86	0.79
D7b	5	8.30	1433	717	9340	14.10	0.00	12.26	1.00	0.59	31.71	0.15	31.78	0.34	0.79
D8	5	9.00	147	74	9620	0.87	0.00	6.03	0.97	0.69	30.90	0.15	31.96	0.56	4.07
D9b	5	8.30	1067	534	9820	4.10	0.00	9.48	1.00	0.62	32.29	0.15	32.02	0.37	0.74
D10b	5	8.30	1300	650	8970	10.14	0.00	10.76	1.00	0.61	31.48	0.15	31.91	0.36	0.59
D11b	25	8.30	1040	520	9090	94.40	0.00	13.71	0.79	0.58	25.33	0.15	25.71	1.16	1.72
D12b	25	8.30	833	417	9030	21.20	0.00	10.93	1.00	0.61	26.63	0.15	27.62	0.27	0.29
D13b	25	8.30	840	420	9210	6.42	0.00	11.18	1.00	0.60	28.09	0.15	27.63	0.27	0.65
D14b	25	8.30	560	280	9220	3.92	0.00	7.46	1.00	0.66	28.66	0.15	27.97	0.29	0.71
D15	25	8.30	293	147	9270	1.01	0.00	3.91	1.00	0.75	29.50	0.15	28.58	0.34	0.82
D16	25	8.30	493	247	9530	6.64	0.00	6.74	1.00	0.67	28.05	0.15	28.06	0.30	0.68
D17	25	8.30	287	144	9590	0.59	0.00	3.95	1.00	0.75	28.30	0.15	28.57	0.34	0.81
D18	25	8.30	313	157	9100	1.19	0.00	4.13	1.00	0.74	28.49	0.15	28.53	0.33	0.81
D19b	25	8.30	1033	517	9470	79.60	0.00	14.07	0.84	0.57	27.58	0.15	26.11	0.99	1.62
D20b	25	8.30	833	417	9540	51.20	0.00	11.41	0.90	0.60	26.97	0.15	26.76	0.73	1.37
D21b	25	8.30	1087	544	9670	87.60	0.00	15.01	0.82	0.57	27.25	0.15	25.94	1.04	1.67
D22b	25	8.30	767	384	9210	54.60	0.00	10.21	0.86	0.61	27.21	0.15	26.55	0.90	1.52
D23	25	8.30	387	194	9450	0.90	0.00	5.26	1.00	0.71	28.08	0.15	28.29	0.31	0.77
D24	40	9.00	67	34	8620	3.56	0.00	4.64	0.60	0.72	24.04	0.15	21.10	3.93	2.18
D25	40	9.00	87	44	8980	3.66	0.00	6.22	0.69	0.68	23.17	0.15	21.80	3.37	2.33
D26	40	9.00	53	27	9660	0.58	0.00	4.03	0.99	0.75	24.77	0.15	25.61	0.34	0.47
D27	40	9.00	107	54	9450	4.24	0.00	7.99	0.71	0.65	20.01	0.15	21.82	3.21	2.37
D28	40	9.00	100	50	9740	1.65	0.00	7.64	0.95	0.65	23.61	0.15	24.58	0.61	1.41
D29	40	9.00	113	57	9310	7.78	0.00	8.34	0.51	0.64	21.57	0.15	19.51	4.31	2.02
D30	40	9.00	100	50	9670	2.46	0.00	7.61	0.86	0.65	22.65	0.15	23.61	1.65	2.11
D31	40	9.00	113	57	9800	3.08	0.00	8.67	0.83	0.64	22.13	0.15	23.17	1.99	2.24
D32	40	9.00	100	50	9680	4.14	0.00	7.6	0.69	0.65	21.65	0.15	21.68	3.34	2.35
D33	40	8.30	247	124	8790	3.42	0.00	3.81	1.00	0.76	25.73	0.15	25.81	0.44	0.74
D34	40	8.30	433	217	4230	2.88	0.00	3.74	1.00	0.76	25.87	0.15	25.83	0.42	0.78
D35	40	8.50	93	47	9610	0.15	0.00	2.42	1.00	0.83	25.70	0.15	26.26	0.48	0.86
D36	40	8.70	160	80	9930	2.22	0.00	6.6	0.99	0.67	24.03	0.15	25.25	0.36	0.27
D37	40	9.60	60	30	19,500	7.94	0.00	19.27	0.16	0.54	15.31	0.15	13.52	3.29	0.61
D38b	40	8.30	547	274	9280	144.40	0.00	8.84	0.41	0.63	24.99	0.15	21.05	2.00	1.12
D39b	40	8.30	480	240	8900	185.20	0.00	7.49	0.30	0.66	24.77	0.15	20.47	1.61	0.98
D40b	40	8.30	213	107	9190	1.23	0.00	3.41	1.00	0.77	25.91	0.15	25.91	0.45	0.80

[a] "B" refers to Baker (2015), "D" refers to Dietzel et al. (2009).
[b] For the experiment of Dietzel et al. (2009), [DIC] was not monitored during calcite precipitation. It is assumed that the average [DIC] during calcite precipitation was 2/3 ± 1/3 of the measured [DIC] at the onset of calcite precipitation (cf. Section 5.1).
[c] Model output parameters.
[d] Calculated using a partial reaction order n_2 of 0.22 (cf. Section 4.2).

temperatures. The inferred n_2 value fits in the lower range of n_2 predicted by Zuddas and Mucci (1998) for a solution with an ionic strength of ~ 0.04 (Fig. 7B). The sensitivity analysis presented in Fig. 7B, and the relatively narrow range in the 'measured' $\alpha_{c/CO_3^{2-}}$ values, confirms previous suggestions that most of the variations in $\alpha_{c/w}$ arise from the $^{18}O/^{16}O$ of the precipitating DIC species (Wang et al., 2013; Watkins et al., 2013, 2014). Understanding how the $\alpha_{c/w}$ is affected by KIE between DIC and water is therefore critical for interpreting the $\delta^{18}O$ of calcite precipitated in CO_2-fed solutions such as in the calcifying fluid of biological calcifiers (McConnaughey, 1989a,b). The following section compares the measured and modelled $\alpha_{c/w}$ for experimental conditions with various degrees of isotopic disequilibrium between the DIC pool and water.

5.3. Calcite precipitated from isotopically non-equilibrated DIC

Kinetic isotope effects related to the CO_2 hydration and hydroxylation reactions produce anomalously low $\alpha_{c/w}$ values relative to calcite precipitated from an equilibrated DIC pool (McConnaughey, 1989b; Clark et al., 1992). However, these kinetic effects have not been fully quantified or integrated in a general isotopic model of calcite growth. Our model estimates the fractionation between calcite and CO_3^{2-} (Section 5.2), and the only model unknown remaining to quantify DIC-H_2O kinetic effects is the kinetic isotope fractionation related to the hydroxylation of CO_2 ($^{18}k_{+4}/^{16}k_{+4}$). One measured $\alpha_{c/w}$ value from an experiment at pH 10.5 and 5 °C (Fig. 8A, experiment D6 in Table 3; Dietzel et al., 2009) can be used to estimate $^{18}k_{+4}/^{16}k_{+4}$ directly due to negligible CO_2 hydration at this pH and the very low level of isotopic equilibration between DIC and H_2O ($E_{DIC} = 0.01$). Our model reproduces the $\alpha_{c/w}$ of experiment D6 at $^{18}k_{+4}/^{16}k_{+4} = 0.9958$ (using $n_2 = 0.22$, Section 5.2). A very similar result ($^{18}k_{+4}/^{16}k_{+4} = 0.9956 \pm 0.0002$) is also obtained by conducting a sensitivity analysis of data-model agreement for the entire dataset of Dietzel et al. (2009) (average $|\Delta^{18}O_{data-model}| = 0.91‰$, $r^2 = 0.89$). Overall, 40 of the 48 measured $\alpha_{c/w}$ values are within error of model outputs (Fig. 8, Table 3), indicating that the model reasonably predicts the oxygen isotope fractionation between $CaCO_3$ and CO_3^{2-} and between CO_3^{2-} and H_2O over a wide range of temperature, pH, Ω and DIC residence times.

Despite the overall good data-model agreement, three $\alpha_{c/w}$ values measured by Dietzel et al. (2009) significantly differ from the modelled $\alpha_{c/w}$ values (D1, D38b, D39b in Table 3) and it is conceivable that these differences are not caused by uncertainties in model input parameters. Potential model limitations include the assumptions of $CaCO_3$ precipitation from an infinite DIC pool and negligible CO_2 escape from the precipitating solution. Both $CaCO_3$ precipitation from a finite DIC pool and CO_2 escape from solution would result in higher $\alpha_{c/w}$ values (Clark and Lauriol, 1992; Kim et al., 2006). Hence, our model would underestimate $\alpha_{CO_3^{2-}/w}$ if the above assumptions are not valid. New calcite growth experiments in CO_2-fed solution without carbonic anhydrase and with a close monitoring of the solution pH, [DIC] and mineral growth rate would help to resolve these issues.

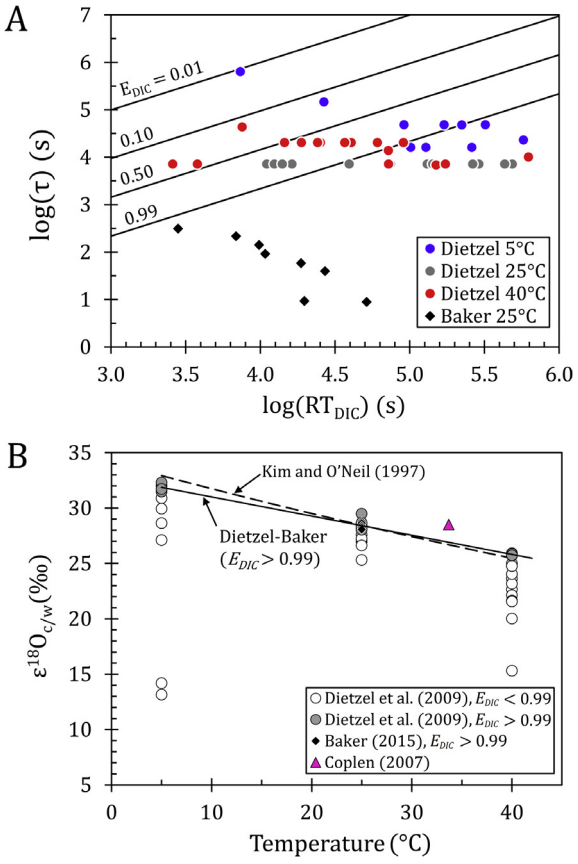

Fig. 6. Level of isotopic equilibrium between the DIC pool and water (E_{DIC}) during the calcite precipitation experiments of Dietzel et al. (2009) and Baker (2015). (A) E_{DIC} calculated as a function of the DIC residence time in solution (RT_{DIC}) and the rate of isotopic equilibration between DIC and water expressed as the time constant τ. Data points represent individual precipitation experiment with E_{DIC} ranging from ~ 0.01 (disequilibrium limit) to more than 0.99 (equilibrium limit). (B) Oxygen isotope fractionation ($\varepsilon_{c/w}$) vs temperature for calcite precipitated from an equilibrated ($E_{DIC} > 0.99$) and non-equilibrated ($E_{DIC} < 0.99$) DIC pool. For a given temperature, and where the DIC pool is isotopically equilibrated, the $\varepsilon_{c/w}$ are restricted to a narrow range of values that are similar to the $\varepsilon_{c/w}$ expected from the relation of Kim and O'Neil (1997).

6. DISCUSSION

6.1. Controls on $\alpha_{c/w}$ where DIC is isotopically equilibrated

The oxygen isotope fractionation between calcite and water ($\alpha_{c/w}$) depends on fractionations between the DIC species and water and fractionations between calcite and

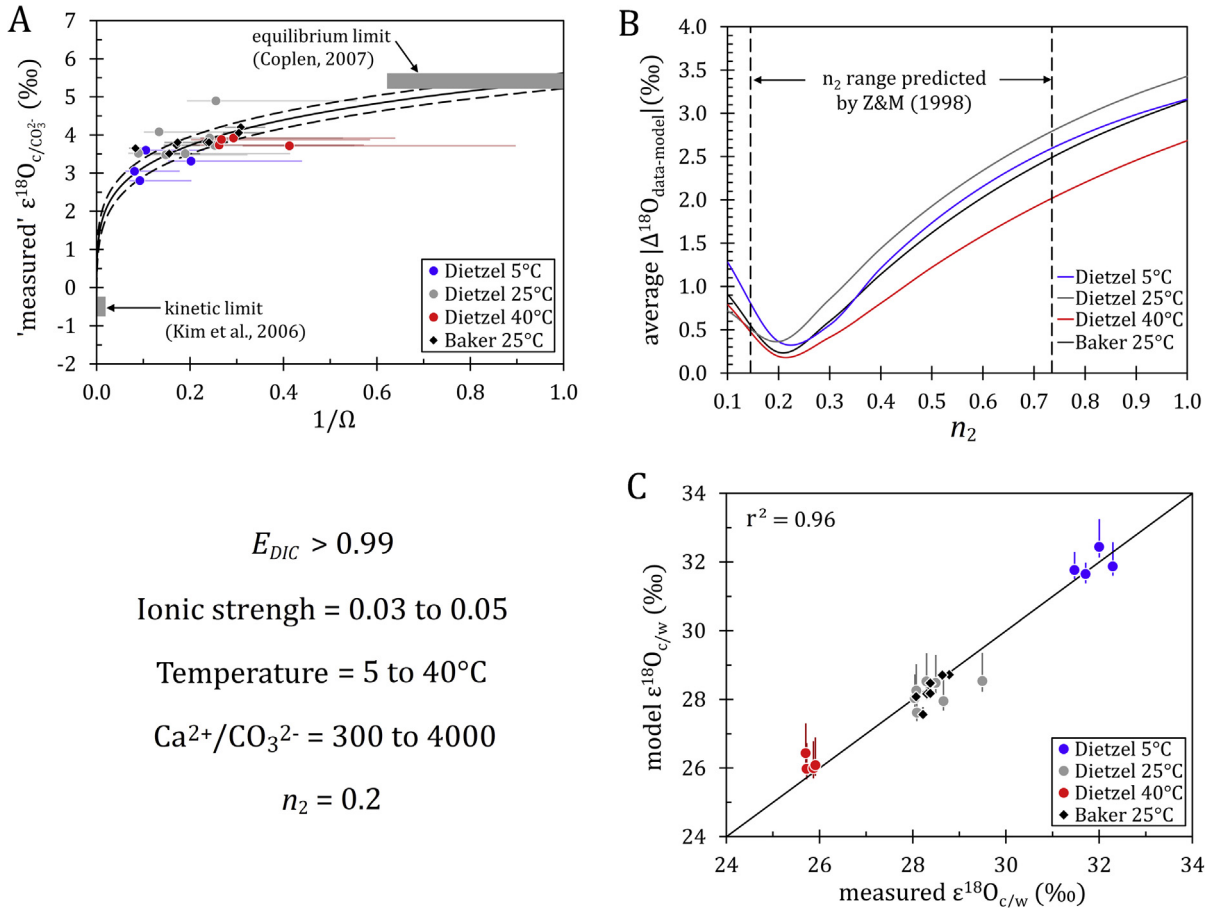

Fig. 7. Measured versus modelled oxygen isotope fractionation between calcite and water for experimental conditions where the DIC pool was isotopically equilibrated. (A) 'Measured' and modelled oxygen isotope fractionation between calcite and CO_3^{2-} ($\varepsilon_{c/CO_3^{2-}}$) versus 1/Ω for the experiments of Dietzel et al. (2009) and Baker (2015). 'Measured' $\varepsilon_{c/CO_3^{2-}}$ values were inferred from oxygen isotope fractionation between calcite and water and the known oxygen isotope fractionation between isotopically equilibrated CO_3^{2-} and water (Beck et al., 2005). Uncertainties in the calcite saturation (Ω) during each precipitation experiment (error bars) are significantly higher for the experiments of Dietzel et al. (2009) than Baker (2015). A model output using $n_2 = 0.22$ shows $\varepsilon_{c/CO_3^{2-}}$ vs 1/Ω (continuous line) with its uncertainties (dashed lines). Modelled $\varepsilon_{c/CO_3^{2-}}$ values assume an equilibrium limit of $+5.5 \pm 0.2$‰ (calculated from Coplen, 2007 and Kluge et al., 2014) and a kinetic limit of -0.5 ± 0.2‰ (calculated from Kim et al., 2006). (B) Sensitivity analysis of the model parameter n_2 (partial reaction order with respect to CO_3^{2-}) showing the best data-model agreement at $n_2 = 0.22 \pm 0.02$ for all experiments and temperatures. This result fits in the lower range of expected n_2 value for solutions with an ionic strength of ~ 0.04 (Zuddas and Mucci, 1998). (C) Modelled versus measured $\varepsilon_{c/w}$ values using $n_2 = 0.22$. Uncertainties on modelled $\varepsilon_{c/w}$ values (error bars) are primarily due to the uncertainties on the solution Ω during calcite precipitation. These figures show that the oxygen isotope fractionation between calcite and the CO_3^{2-} pool ($\varepsilon_{c/CO_3^{2-}}$) is independent of temperature. The solution Ω seems to have a weak negative effect on $\varepsilon_{c/CO_3^{2-}}$, with $\varepsilon_{c/CO_3^{2-}}$ decreasing from +4.1‰ to +2.9‰ between the 3 and 12 range in Ω (i.e. 0.4–0.1 range in 1/Ω).

the DIC species involved in calcite growth (Watkins et al., 2013). In the simplest case where the DIC pool is isotopically equilibrated with water and for a given temperature, the fractionation between each DIC species and water remain constant. In this case, $\alpha_{c/w}$ only depends on surface reaction-controlled kinetics between calcite and the precipitating DIC species (DePaolo, 2011; Watkins et al., 2013, 2014). Measured $\alpha_{c/w}$ values for experimental conditions where calcite precipitated from an isotopically equilibrated pool show temperature-independent variations of more than 1.0‰ (Fig. 7A), suggesting that one or more parameter, other than temperature, affects fractionation at the mineral/water interface.

There are competing hypotheses to explain the variability of $\alpha_{c/w}$ under these conditions: (1) $\alpha_{c/w}$ decreases as pH increases due to a shift from HCO_3^- to CO_3^{2-} as the dominant adsorbed ions onto the growing calcite surface (Watkins et al., 2014), (2) $\alpha_{c/w}$ is shifted towards lower values due to a competition between calcite surface growth rate and diffusive processes in the inner crystal region (Watson, 2004), and (3) $\alpha_{c/w}$ is shifted towards lower values due to an increase in calcite precipitation rate relative to calcite dissolution rate with increasing Ω (this study). These hypotheses can be tested against the experimental data of Dietzel et al. (2009) and Baker (2015) since the solution pH, DIC speciation, Ω and the net calcite growth rate are

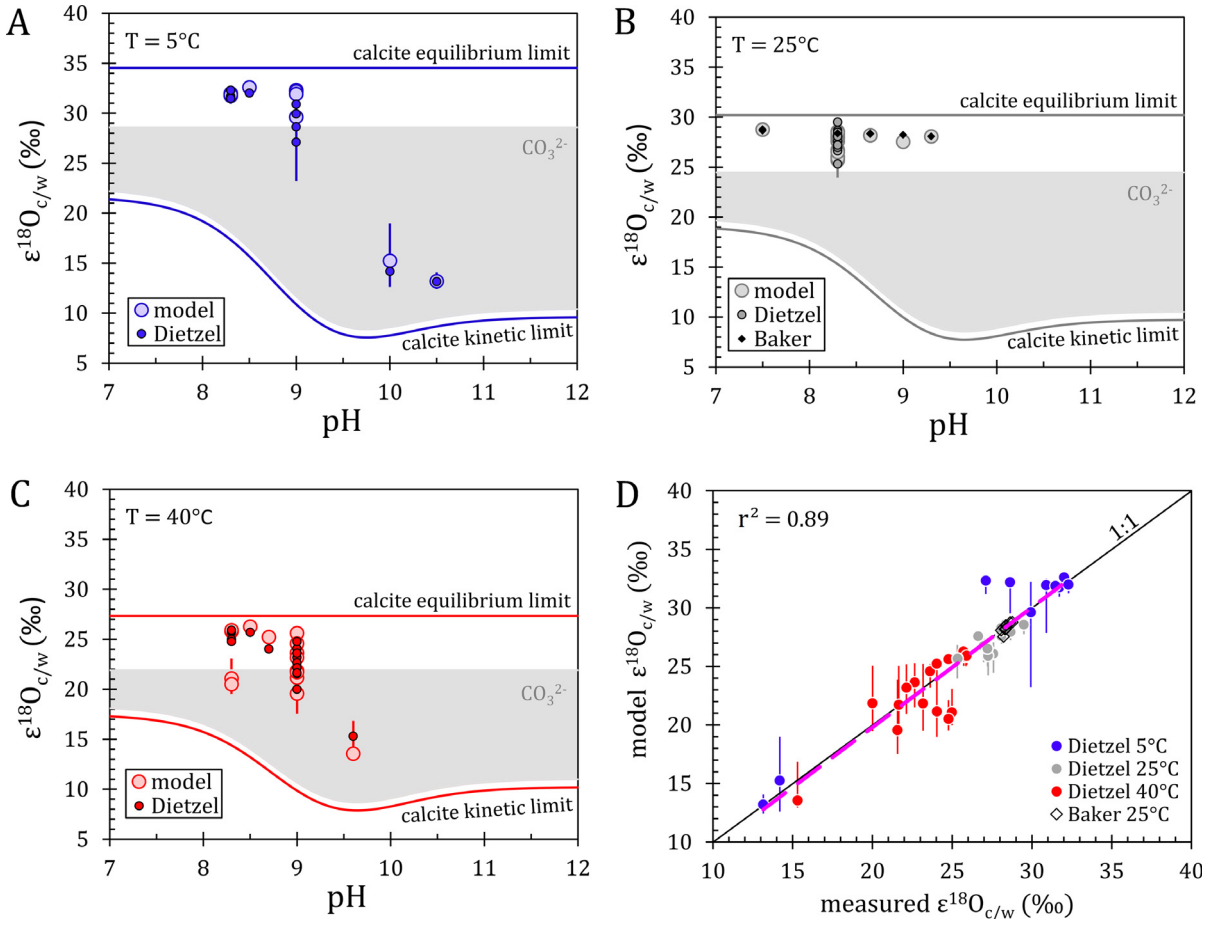

Fig. 8. Measured versus modelled oxygen isotope fractionation between calcite and water ($\varepsilon_{c/w}$) for all experimental conditions at (A) 5 °C, (B) 25 °C and (C) 40 °C. The experimental data include all the $\varepsilon_{c/w}$ values presented in Fig. 7 and additional $\varepsilon_{c/w}$ values from the experiments of Dietzel et al. (2009) where calcite precipitated from non-isotopically equilibrated DIC (cf. Fig. 6). Modelled $\varepsilon_{c/w}$ values depend on the oxygen isotope fractionation between CO_3^{2-} and water ($\varepsilon_{CO_3^{2-}/w}$) and the oxygen isotope fractionation between calcite and CO_3^{2-} ($\varepsilon_{c/CO_3^{2-}}$). All modelled $\varepsilon_{c/w}$ were calculated using a partial reaction order n_2 value of 0.22 (cf. Fig. 7 and Section 5.2). The model assumes that the equilibrium limit of $\varepsilon_{c/w}$ (upper horizontal line) is independent of pH while the kinetic limit of $\varepsilon_{c/w}$ depends on the CO_2 hydroxylation to CO_2 hydration reaction rate ratio, which depends on pH (lower curved line). At any pH, the difference between the equilibrium and kinetic limit of $\varepsilon_{CO_3^{2-}/w}$ (grey shaded area) and $\varepsilon_{c/w}$ (straight and curves lines) decreases with temperature. (D) Compilation of measured versus modelled $\varepsilon_{c/w}$ values at 5 °C, 25 °C and 40 °C temperatures. A linear regression between modelled and measured $\varepsilon_{c/w}$ values (pink dash line) yields an r^2 value of 0.89. In each plot, uncertainties on modelled $\varepsilon_{c/w}$ values (error bars) were calculated as the square root of the sum of square uncertainties from each model input parameter (cf. Appendix A.8). The good data-model agreement suggests that kinetic isotope effects between DIC and H_2O and between calcite and CO_3^{2-} are well predicted by the model.

reasonably well constrained, and because it is possible to identify those experiments for which the DIC pool was isotopically equilibrated (Fig. 6, Table 3).

In the study of Baker (2015), $\alpha_{c/w}$ decreases by ~ 0.7‰ between pH 7.5 and 9.3 (Fig. 9A). This pH dependence is less pronounced than the previously reported value of ~ 1.6‰ between pH 7.7 and 9.3 (Watkins et al., 2014). Although the Watkins et al. (2014) model can reproduce either of these pH dependencies by ascribing the $\alpha_{c/w}$ variations to an increasing contribution of HCO_3^- with decreasing pH (Fig. 9A and B), the model cannot reproduce the results of Dietzel et al. (2009), which exhibit $\alpha_{c/w}$ variations of 1.5‰ at the single pH value of 8.3 (Fig. 9A). As noted previously, the Watkins et al. (2014) model uses the value of $\alpha^{eq}_{CO_3^{2-}/w} = 1.0268$ (at 25 °C) from Wang et al. (2013), which is significantly higher than the $\alpha^{eq}_{CO_3^{2-}/w}$ value of 1.0245 (at 25 °C) from Beck et al. (2005). Using the latter value with the Watkins et al. (2014) model results in a significant overestimation of the pH dependence of $\alpha_{c/w}$ (not shown). It is possible that HCO_3^- does not contribute as directly to the oxygen isotope budget of calcite (via attachment followed by deprotonation) as indicated by the ion-by-ion model of Watkins et al. (2014). This conclusion is supported by inorganic aragonite precipitation experiments, which show no significant pH effect on the oxygen isotope fractionation between rapidly precipitated aragonite and water (Kim et al., 2006). Based on these considerations, our current thinking is that CO_3^{2-} is the main contributing DIC species to calcite and aragonite growth,

even at pH values where HCO_3^- is by far the dominant species in solution.

In the model of Watson (2004), the level of isotopic equilibration is determined by a competition between calcite growth rate and diffusive processes on the solid side of the solid-fluid interface. The prediction is that $\alpha_{c/w}$ should decrease systematically with increasing net calcite growth rate, yet we observe no apparent relationship for growth rates varying from 0.05 to 1.05 μmol/m^2/s (Fig. 9C). The Watson (2004) model does not make predictions regarding solution ionic strength and does not account for isotopic effects arising on the aqueous side of the solid-fluid interface, such as mass-dependent ion desolvation rates, that are likely significant (Hofmann et al., 2012; Watkins et al., 2017).

In the model presented in this study, CO_3^{2-} is the only precipitating DIC species and the fractionation between calcite and CO_3^{2-} ($\alpha_{c/CO_3^{2-}}$) is determined by the r_{-c}/r_{+c} ratio, which in turn is a function of the solution Ω and ionic strength through the partial reaction order n_2 (Section 4.2). This model therefore predicts that $\alpha_{c/w}$ should decrease with increasing Ω where calcite precipitates from an isotopically equilibrated DIC pool. Measured $\alpha_{c/w}$ values appear inversely related to Ω (Fig. 7A and 9D), although the uncertainties in Ω are relatively large. A more systematic relationship may emerge with additional experiments in which calcite is grown in solutions near chemical equilibrium and in solutions that are highly supersaturated. Importantly, if CO_3^{2-} is the only precipitating DIC species, $\alpha_{c/w}$ should be insensitive to pH when Ω is constant. The systematic pH dependence on $\alpha_{c/w}$ observed in previous studies (Watkins et al., 2014; Baker, 2015) may in fact be due to a systematic increase in Ω with increasing pH in those experiments (Table 3). Another expectation from our model is that increasing ionic strength should push the system towards the kinetic limit (Eq. (16)) and lead to larger $CaCO_3$-

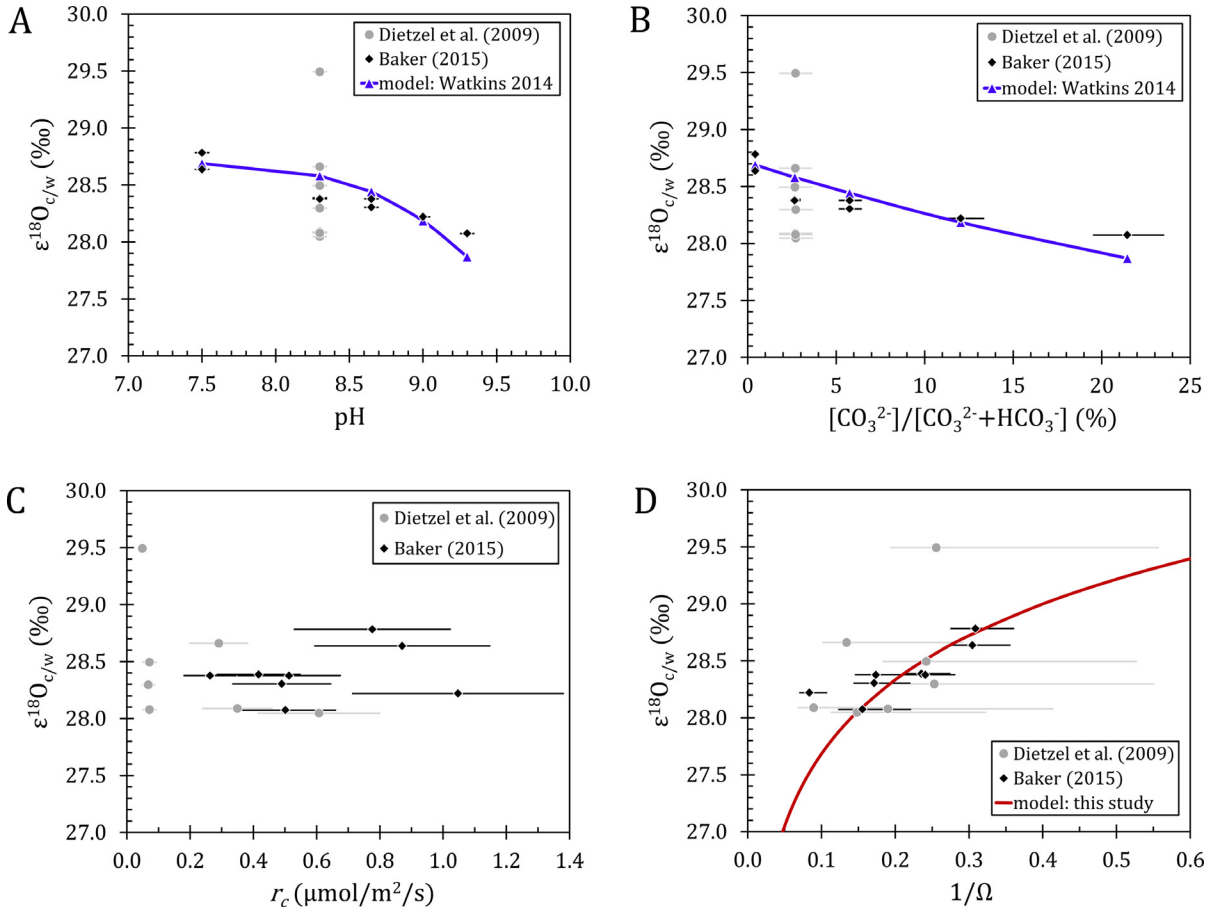

Fig. 9. Measured oxygen isotope fractionation between calcite and water ($\varepsilon_{c/w}$) at 25 °C for experimental conditions with isotopically equilibrated DIC (data from Dietzel et al., 2009 and Baker, 2015). (A) $\varepsilon_{c/w}$ vs pH. (B) $\varepsilon_{c/w}$ vs the relative proportion of CO_3^{2-} and HCO_3^- in solution. (C) $\varepsilon_{c/w}$ vs the calcite growth rate (normalized to the calcite surface area). (D) $\varepsilon_{c/w}$ vs calcite saturation state (1/Ω). Also shown for comparison are model outputs form the Watkins et al. (2014) model (panel A and B; computed with $\alpha^{+c}_{c/CO_3^{2-}} = 0.9995$ and $\alpha^{+c}_{c/HCO_3^-} = 0.9967$) and the model presented in this study (panel D; computed with $\alpha^{+c}_{c/CO_3^{2-}} = 0.9995$ and $n_2 = 0.22$). The Watkins et al. (2014) model agrees with measured $\varepsilon_{c/w}$ from Baker (2015) but cannot reproduce the scatter of the Dietzel et al. (2009) data. The model presented in this study potentially explains the measured $\varepsilon_{c/w}$ from both Baker (2015) and Dietzel et al. (2009).

CO_3^{2-} fractionations. This hypothesis can be tested with experiments at constant Ω but variable ionic strength.

6.2. Controls on $\alpha_{c/w}$ where DIC is isotopically non-equilibrated

Measured $\alpha_{c/w}$ values for slowly and rapidly precipitated calcite in the absence of carbonic anhydrase decrease by as much 19‰ where the solution pH increases from ~ 8.5 to 10.0 (Fig. 8A, Dietzel et al., 2009). This decrease in $\alpha_{c/w}$ cannot be attributed to a change in the contribution of DIC species to calcite growth since DIC speciation does not significantly affect $\alpha_{c/w}$ when the DIC is isotopically equilibrated (Section 6.1). The strong pH dependence of $\alpha_{c/w}$ is therefore related to disequilibrium isotope effects between CO_3^{2-} and water that are related to the hydration and hydroxylation of CO_2 (McConnaughey, 1989b; Usdowski and Hoefs, 1990; Clark et al., 1992; Dietzel et al., 1992). In this case, CO_3^{2-} (partially) inherits the $^{18}O/^{16}O$ of CO_2, H_2O and OH^- and the fractionation between $CO_3^{2-}$and water ($\alpha_{CO_3^{2-}/w}$) decreases with pH because (1) the rate of isotopic exchange between the DIC species and water decreases with increasing pH, and (2) the CO_2 hydroxylation reaction rate increases with pH, lowering the initial $^{18}O/^{16}O$ of HCO_3^- and CO_3^{2-} (Fig. 5) because OH^- has a low $^{18}O/^{16}O$ value relative to H_2O (−39‰ at 25 °C, Green and Taube, 1963). In other words, strong KIE between CO_3^{2-} and H_2O are more likely at high pH, and the KIFF related to the conversion of CO_2 to HCO_3^- and CO_3^{2-} increases with pH (Figs. 5 and 8).

The 19‰ and 11‰ variations in measured $\alpha_{c/w}$ at 5 °C and 40 °C reported by Dietzel et al. (2009) are explained almost entirely by the variations in the $^{18}O/^{16}O$ of the CO_3^{2-} pool (Fig. 8, grey shaded area), supporting the idea that the fractionation between calcite and CO_3^{2-} is not significantly affected by the solution temperature and pH. Another notable model result supported by the experimental data is the reduction of the difference between the equilibrium and kinetic limits of $\alpha_{CO_3^{2-}/w}$ (and $\alpha_{c/w}$) with increasing temperature. This is explained by the decrease of the CO_3^{2-}-water equilibrium fractionation factor ($\alpha^{eq}_{CO_3^{2-}/w}$) with temperature but a limited temperature sensitivity on the initial $^{18}O/^{16}O$ of hydrated and hydroxylated CO_2.

This study focuses on KIE during CO_2 hydration and hydroxylation, however opposite KIE (i.e. ^{18}O enrichment of the DIC pool) are known to occur during the reverse reactions of CO_2 dehydration and dehydroxylation (Clark and Lauriol, 1992). These latter KIE are likely to affect the $^{18}O/^{16}O$ of $CaCO_3$ where precipitation follows rapid CO_2 degassing such as during the formation of cave calcite (Hendy, 1971). The degassing of CO_2 elevates the solution pH, which causes the dehydration of carbonic acid and shifts the DIC speciation towards carbonate ions. Hence, we predict that in addition to the KIE related to the CO_2 dehydration/dehydroxylation reactions, HCO_3^- deprotonation also contributes to the ^{18}O enrichment of the CO_3^{2-} pool (and $CaCO_3$) during CO_2 degassing (see Section 4.2.4).

7. IMPLICATIONS

7.1. The equilibrium limit of $\alpha_{c/w}$

For about two decades, the $\alpha_{c/w}$ versus temperature relationship proposed by Kim and O'Neil (1997) (KO97) was widely used to assess isotopic equilibrium in biogenic calcite (e.g. Bemis et al., 1998; von Grafenstein et al., 1999; Barras et al., 2010; Candelier et al., 2013; Marchitto et al., 2014; Rollion-Bard et al., 2016 and many others). However, in the KO97 experiments calcite precipitation was triggered by CO_2 degassing, which can increase the $^{18}O/^{16}O$ of DIC and $CaCO_3$ (Section 6.2). If the rate of calcite precipitation outpaces the rate of isotopic equilibration between the DIC species and water, then the $\alpha_{c/w}$ will reflect the isotopic disequilibrium between the DIC and water (Watkins et al., 2013). Interestingly, KO97 reported a 1–2‰ increase in $\alpha_{c/w}$ with increasing Ca^{2+} and DIC concentration and thus with increasing Ω. This is the opposite pattern expected for calcite precipitating from an isotopically equilibrated DIC pool (cf. Section 4.2, Fig. 7A). We postulate that the positive relationship between $\alpha_{c/w}$ and Ω reported by KO97 is due to a negative correlation between Ω and the DIC residence time in solution. The time available for DIC-H_2O isotopic equilibration likely decreases with Ω because the rate of calcite precipitation commonly increases with the solution Ω. As a result, KIE between DIC and H_2O are likely to increase with Ω. Another supporting observation for the imprint of DIC-H_2O kinetic isotope effects on $\alpha_{c/w}$ during the KO97 experiments is the reducing effect of Ω on $\alpha_{c/w}$ with increasing temperature (cf. Fig. 6 in Kim and O'Neil, 1997). DIC-H_2O kinetic isotope effects should decrease with increasing temperature because the isotopic exchange rate between DIC and water increases significantly with temperature. Finally, based on reported Ca^{2+} and HCO_3^- concentrations of 5 mM for the less concentrated solution of KO97 and a pH of 7.6–8.2, a Ω of 7–40 is estimated for the precipitating solutions. It is unlikely that isotopic equilibrium between calcite and carbonate ions would have been reached at these high Ω values (i.e. calcite precipitated in conditions far from chemical equilibrium). Hence, the $\alpha_{c/w}$ reported by Kim and O'Neil (1997) most likely reflects KIE between calcite and CO_3^{2-} and perhaps KIE between CO_3^{2-} and H_2O.

Based on theoretical constraints presented in Section 4.2 and Fig. 3 (i.e. isotopic equilibrium is approached in solution of low Ω and low ionic strength), we support previous suggestions that the natural inorganic calcite from Devils Hole cave system formed near isotopic equilibrium conditions (Coplen, 2007; Watkins et al., 2013; Kluge et al., 2014). However, the calculated (near) equilibrium value of $\alpha_{c/w}$ at Devils Hole (1.02849 at 33.7 °C, Coplen, 2007) remains poorly constrained because of uncertainties in the water temperature (± 2.6 °C, Kluge et al., 2014) and water $\delta^{18}O$ value at time of calcite growth approximately 4000 years ago. Moreover, the temperature sensitivity of equilibrium $\alpha_{c/w}$ has yet to be determined accurately, since data from Devils Hole is limited to a single temperature of calcite precipitation. Hence, new experimental determi-

nations of equilibrium $\alpha_{c/w}$, especially at lower temperature (5–20 °C), would help resolve discrepancies in equilibrium $\alpha_{c/w}$ estimates. Such experiments should take advantage of the hypotheses presented herein regarding the effect of the solution Ω and ionic strength on the isotopic equilibration between $CaCO_3$ and CO_3^{2-}.

7.2. Oxygen isotope "vital effects" in biogenic $CaCO_3$

Deviations in ^{18}O among biogenic $CaCO_3$ (e.g. corals, foraminifers, coccolithophores, ostracods, molluscs, urchins) and inorganic calcite or aragonite precipitated in the same environmental conditions are due to biologically induced modifications of the carbonate chemistry in the calcifying fluid (CF) relative to the external environment (e.g. McConnaughey, 1989a; Rollion-Bard et al., 2003; Ziveri et al., 2012; Hermoso et al., 2016; Devriendt et al., 2017). These "vital effects" in ^{18}O vary between taxonomic groups and are thought to originate from (1) kinetic isotope effects related to the contribution of metabolic CO_2 to the precipitating DIC pool (McConnaughey, 1989a; Rollion-Bard et al., 2003; Hermoso et al., 2016), and/or (2) a CF with an elevated pH relative to that of the surrounding water (Adkins et al., 2003; Rollion-Bard et al., 2003; Ziveri et al., 2012; Devriendt et al., 2017). Another potential factor contributing to oxygen isotope vital effects is the formation of amorphous calcium carbonate (ACC) and subsequent transformation to a $CaCO_3$ polymorph (Dietzel et al., 2015) but this is not investigated here due to the absence of published isotopic data.

The model presented in this study can be used to test hypothesis (1) and (2) for different groups of organisms, since it integrates kinetic isotope effects arising from the dissolution of CO_2 in water coupled with the effect of pH on isotopic fractionations in the $CaCO_3$-DIC-H_2O system. Here we focus on foraminifers and corals because the calcifying fluid pH (pH_{cf}) of these organisms has been measured directly with microelectrodes and/or pH sensitive dyes (foraminifers: Jorgensen et al., 1985; Rink et al., 1998; Köhler-Rink and Kühl, 2005; Bentov et al., 2009; de Nooijer et al., 2009; tropical corals: Al-Horani et al., 2003; Venn et al., 2011; Cai et al., 2016). These studies showed that for both foraminifers and corals, calcification takes place in a closed or semi-closed environment with an elevated pH_{cf} relative to that of seawater and a DIC residence time in the CF that is very short (i.e. seconds to minutes). For foraminifers, the pH_{cf} (seawater scale) is 8.8 ± 0.2 while tropical corals have pH_{cf} values ranging from 8.5 to 9.5. An elevated pH_{cf} for corals is also supported by $\delta^{11}B$ measurements of coral skeletons (Allison and Finch, 2010b; Rollion-Bard et al., 2011; McCulloch et al., 2012; Allison et al., 2014) but uncertainties regarding the mode of boron incorporation in $CaCO_3$ limit the accuracy of the $\delta^{11}B$ pH-proxy (Foster and Rae, 2016). Thus only direct pH_{cf} measurements are considered here. With knowledge of the pH_{cf} values, the remaining unknown model parameters to simulate the $^{18}O/^{16}O$ of the DIC in the CF (DIC_{cf}) of foraminifers and corals are the sources of DIC_{cf} (metabolic CO_2 vs DIC from seawater) and the activity of the enzyme carbonic anhydrase in the CF (Uchikawa and Zeebe, 2012). Assuming minimal oxygen isotopic fractionation between $CaCO_3$ and the DIC_{cf} due to the short DIC_{cf} residence time and slow rate of DIC-H_2O isotopic equilibration in the high pH calcifying fluid environment (cf. Usdowski et al., 1991; Uchikawa and Zeebe, 2012), $\alpha_{c/w}$ is simulated for $CaCO_3$ precipitating at 25 °C in a seawater-like solution (i.e. salinity = 35 g/kg, [DIC] = 2 mmol/kg, $[Ca^{2+}]$ = 10 mmol/kg) as a function of pH_{cf} and under the following scenarios:

(a) the DIC_{cf} pool is at isotopic equilibrium with water prior to a rapid precipitation of DIC ($E_{DIC} \sim 1$, 'Zeebe, 1999' and 'Adkins et al., 2003' scenarios),
(b) the DIC_{cf} pool derives exclusively from dissolved CO_2, and a short residence time of DIC_{cf} in solution prevents DIC_{cf}-H_2O isotopic equilibration ($E_{DIC} \sim 0$, 'McConnaughey, 1989b' scenario),
(c) same as (b) but with a carbonic anhydrase activity in the calcifying fluid within the 5–100 s^{-1} range (i.e. as measured in the tissues of *Porites* corals, Hopkinson et al., 2015).

Note that scenario (a) leads to the same model results for systems with and without carbonic anhydrase in solution since the equilibrium oxygen isotopic composition of DIC is independent of the presence/absence of carbonic anhydrase (Uchikawa and Zeebe, 2012). It is also important to realize that the small and closed calcifying fluid of foraminifers and corals is not analogous to the open system simulations presented in Section 5 where the DIC residence time in solution is in the order of hours to days (Fig. 6A) and where DIC precipitation is not quantitative. A slow precipitation of $CaCO_3$ in open system conditions leads to a significant isotopic fractionation between $CaCO_3$ and CO_3^{2-} (and DIC) while a fast and quantitative precipitation of DIC in a closed system results in no isotopic fractionation between $CaCO_3$ and DIC (cf. McCrea, 1950; Beck et al., 2005; Kim et al., 2006, 2014). The 'closed system and quantitative DIC precipitation' assumption for the CF of corals and foraminifers does not compromise the physical basis of our inorganic model: namely that CO_3^{2-} is the dominant DIC species contributing to $CaCO_3$ growth. In fact, within a high and regulated pH environment such as in the CF of corals and foraminifers, consumed CO_3^{2-} ions during $CaCO_3$ growth would be constantly replaced by deprotonated HCO_3^- to maintain the chemical equilibrium imposed by the regulated pH environment. Hence, a DIC pool may be quantitatively consumed without a direct contribution of HCO_3^- ions to calcite growth (Fig. 4, Eq. (30)). Because DIC-H_2O isotopic exchanges are very slow at high pH (Usdowski et al., 1991; Beck et al., 2005; Uchikawa and Zeebe, 2012), the newly formed CO_3^{2-} ions would likely retain the $^{18}O/^{16}O$ of the HCO_3^- ions and hence the resulting $\delta^{18}O_c$ would reflect the $^{18}O/^{16}O$ of the DIC in solution (Kim et al., 2006; Fig. 4). In other words, HCO_3^- ions contribute to the $^{18}O/^{16}O$ of a precipitating carbonate mineral where these ions deprotonate in solution (e.g. due to an increase in solution pH) and the newly formed CO_3^{2-} ions are incorporated

into $CaCO_3$ before reaching isotopic equilibrium with H_2O. Finally, since we assume that biogenic $CaCO_3$ reflects the $^{18}O/^{16}O$ of DIC in the calcifying fluid, modelling outputs are independent of the $CaCO_3$ mineral (e.g. calcite vs aragonite).

A comparison of model outputs with biogenic oxygen isotope data (Fig. 10A) shows that scenario (a) agrees with the $_{c/w}$ of the planktic foraminifers *Orbulina universa* and *Globigerina bulloides* ($_{c/w}$ = 28.7‰ at 25 °C, calculated from Bemis et al., 1998) and the benthic foraminifer *Cibicidoides* ($_{c/w}$ = 28.9‰ at 25 °C, calculated from Marchitto et al., 2014) at the measured pH_{cf} value of 8.8 ± 0.2. Note that the $_{c/w}$ of planktic and benthic foraminifers cannot be explained by a quantitative precipitation of external seawater DIC (i.e. the Zeebe (1999) model, which is equivalent to scenario (a) at pH 8.1 ± 0.1) or by either scenarios (b) or (c). If the ^{18}O of foraminifers reflects the $^{18}O/^{16}O$ of an internal DIC pool that is isotopically equilibrated (scenario (a) at pH_{cf} 8.8), then any changes in the pH_{cf} should affect the foraminifer ^{18}O value. The ^{18}O of planktic foraminifers decreases with increasing seawater pH (Spero et al., 1997), which together with our model results suggests that the internal calcifying fluid of planktic foraminifers is dependent on the external seawater pH. Another important point is that the reasonable agreement in $_{c/w}$ values between foraminiferal calcite and the inorganic calcite from the Kim and O'Neil (1997) experiments (KO97, light blue line in Fig. 10) could be coincidental since the $_{c/w}$ expected from the KO97 equation is very similar to the DIC-H_2O fractionation factor ($_{DIC/w}$) at pH 8.8 and salinity 35.

The low $_{c/w}$ of coral aragonite ($_{c/w}$ = 25.4–27.1‰ at 25 °C, for *Porites*, calculated from Felis et al., 2003, 2004; Suzuki et al., 2005 and Omata et al., 2008) compared to that of foraminiferal calcite can be explained by scenario (a) at a pH of 9.5, a combination of scenario (a) and (b) (i.e. partially equilibrated DIC) or by scenario (c). Since carbonic anhydrase is thought to be present in the coral calcifying fluid (Tambutté et al., 2007; Bertucci et al., 2013; Hopkinson et al., 2015), scenario (a) and (c) may be the most realistic scenarios for corals. Scenario (a) and (c) are further tested against coral data in Section 7.3.

7.3. The temperature sensitivity of $\delta^{18}O_c$

The temperature dependence of $\delta^{18}O_c$ (and $\alpha_{c/w}$) for slowly precipitated inorganic calcite and aragonite averages

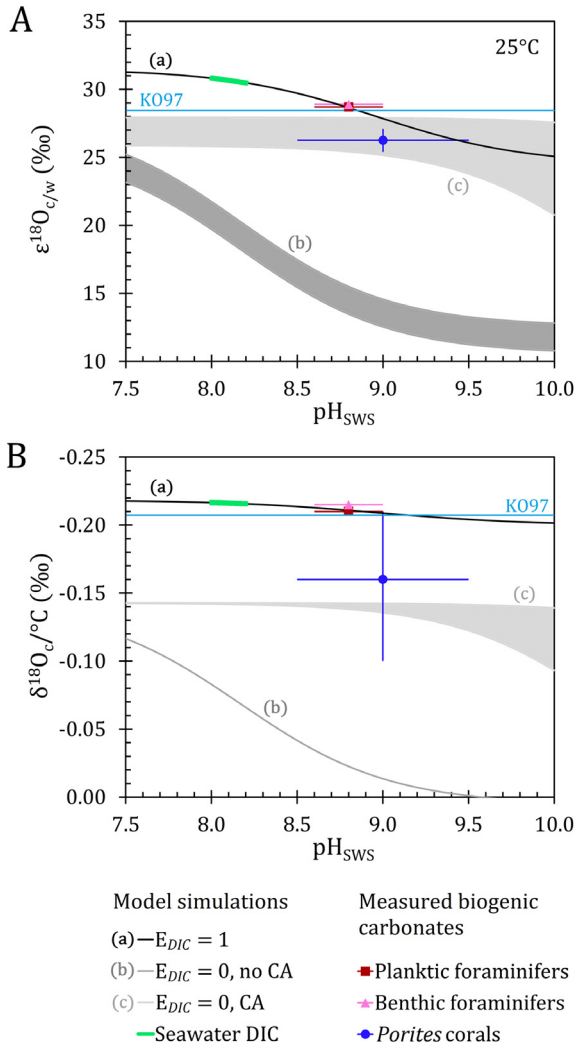

Fig. 10. Comparison of modelled and measured biogenic $CaCO_3$ oxygen isotope data. (A) Oxygen isotope fractionation between $CaCO_3$ and H_2O (expressed in ‰ as $\varepsilon_{c/w}$) at 25 °C and as a function of pH_{SWS} (seawater scale). (B) Average temperature sensitivity of $CaCO_3$ $\delta^{18}O$ ($\delta^{18}O_c$) between 0 and 30 °C as a function of pH_{SWS}. Model outputs are compared to data from planktic foraminifers *Orbulina universa* and *Globigerina bulloides* (Bemis et al., 1998), benthic foraminifer *Cibicidoides* (Marchitto et al., 2014) and *Porites* corals (panel A: calculated from Felis et al., 2003, 2004; Suzuki et al., 2005; Omata et al., 2008; panel B: Gagan et al., 2012). The calcifying fluid pH_{SWS} is 8.8 ± 0.2 for foraminifers (Jorgensen et al., 1985; Rink et al., 1998; Köhler-Rink and Kühl, 2005; Bentov et al., 2009; de Nooijer et al., 2009) and 9.0 ± 0.5 for tropical corals (Al-Horani et al., 2003; Venn et al., 2011; Cai et al., 2016). Simulations were performed assuming a quantitative precipitation of the DIC pool and for different scenarios: (a) $CaCO_3$ precipitates from an isotopically equilibrated DIC pool (E_{DIC} = 1), (b) $CaCO_3$ precipitates from a DIC pool that is not isotopically equilibrated (E_{DIC} = 0) and all the DIC derives from hydrated and hydroxylated CO_2, (c) same as (b) but the enzyme carbonic anhydrase increases the rate of CO_2 hydration by a factor of 100–2000, as in the tissues of *Porites* corals (Hopkinson et al., 2015). For the simulations (b) and (c), shaded areas include uncertainties in the CO_2 hydration/hydroxylation fractionation factors and carbonic anhydrase activity. All simulations were performed with salinity = 35 g/kg, $[Ca^{2+}]$ = 10 mmol/kg and [DIC] = 2 mmol/kg. The $\varepsilon_{c/w}$ and temperature sensitivity of $\delta^{18}O_c$ expected from the expression of Kim and O'Neil (1997) (KO97, light blue line) are shown in panel A and B for comparison. These diagrams suggest that the calcite secreted by planktic and benthic foraminifers formed from a (near) isotopically equilibrated DIC pool, while the aragonite secreted by shallow corals is best explained by the precipitation of non- to partially isotopically equilibrated DIC deriving from hydrated CO_2.

-0.22 ± 0.02‰/°C between 0 and 30 °C (O'Neil et al., 1969; Kim and O'Neil, 1997; Kim et al., 2007; Watkins et al., 2013; this study). There are suggestions that the temperature dependence of $\delta^{18}O_c$ is caused by the effect of temperature on the $^{18}O/^{16}O$ of CO_3^{2-} and HCO_3^-, based on the similar temperature sensitivities of $\alpha_{c/w}$, $\alpha_{CO_3^{2-}/w}$ and $\alpha_{HCO_3^-/w}$ (Wang et al., 2013). Our investigation of the calcite-CO_3^{2-} oxygen isotope fractionation ($\alpha_{c/CO_3^{2-}}$; Fig. 7) shows for the first time that $\alpha_{c/CO_3^{2-}}$ is not significantly affected by temperature, implying that the temperature dependence of $\alpha_{c/w}$ originates from the CO_3^{2-}-H_2O fractionation step rather than the calcite-CO_3^{2-} fractionation step. An important implication of our result is that the temperature dependence of $\alpha_{CO_3^{2-}/w}$ and $\alpha_{c/w}$ should deviate from -0.22 ± 0.02‰/°C when the precipitating CO_3^{2-} ions are not isotopically equilibrated with water. On the other hand, isotopic disequilibrium effects between calcite and CO_3^{2-} should have limited impact on the temperature sensitivity of $\alpha_{c/w}$. This explains why the $\delta^{18}O$ from many biogenic carbonates (e.g. foraminifers, ostracods, coccolithophores) display similar temperature sensitivities despite the carbonates forming in conditions far from isotopic equilibrium (e.g. Xia et al., 1997; Bemis et al., 1998; Chivas et al., 2002; Barras et al., 2010; Candelier et al., 2013; Marchitto et al., 2014; Devriendt et al., 2017).

Fig. 10B shows modelled average temperature sensitivities for $\delta^{18}O_c$ between 0 and 30 °C as a function of pH for calcite precipitating in seawater under the three scenarios described in Section 7.2 (scenario (a): DIC is isotopically equilibrated; scenario (b): DIC derives from CO_2 and is not isotopically equilibrated; scenario (c): same as (b) but with carbonic anhydrase in solution). Under scenario (a), the temperature sensitivity of $\delta^{18}O_c$ is -0.21 ± 0.01‰/°C and is not significantly dependant on pH because the equilibrium $\varepsilon_{CO_3^{2-}/w}$ and $\varepsilon_{HCO_3^-/w}$ values are similar (−0.20‰/°C and −0.22‰/°C respectively, Beck et al., 2005). The good agreement between scenario (a) and foraminiferal data further support the notion that foraminifers precipitate calcite from an isotopically equilibrated DIC pool. Hence, the $\delta^{18}O$-thermometer should work well with foraminiferal calcite as long as the carbonate chemistry of the CF remained similar between specimens from the same species.

Under scenario (b) and (c), the temperature dependences of $\delta^{18}O_c$ are lower than for scenario (a) due to the isotopic imprint from the contributions of oxygen atoms from H_2O and OH^- during the CO_2 hydration and hydroxylation reactions (pathway (31) and (32), Section 4.3.3). In both scenarios (b) and (c), $\delta^{18}O_c$ becomes less sensitive to temperature at high pH values because of the increasing contribution of oxygen atoms from OH^- to the initial isotopic composition of the DIC. As opposed to the $^{18}O/^{16}O$ of CO_2, HCO_3^- and CO_3^{2-}, the $^{18}O/^{16}O$ of OH^- ions increases with increasing temperature (Green and Taube, 1963), leading to an overall reduced temperature effect on the initial $^{18}O/^{16}O$ of DIC derived from hydroxylated CO_2. Interestingly, scenario (b) and (c) may explain why the temperature sensitivity of *Porites* $\delta^{18}O$ (−0.11‰/°C to −0.22‰/°C; Gagan et al., 2012) is lower and more variable than for foraminiferal calcite (−0.21 ± 0.1‰/°C, Bemis et al., 1998; Marchitto et al., 2014). Combining the model results from Fig. 10A and B suggests that the coral data is best explained by scenario (c). Hence, it is postulated that the hydration of metabolic CO_2 in the coral calcifying fluid is the dominant mechanism causing the anomalously low coral $\delta^{18}O$ values and reduced coral $\delta^{18}O$-temperaure sensitivity compared to that of other marine calcifiers.

Overall, the model results suggest that inorganic processes are sufficient to explain oxygen isotope "vital effects" in foraminifers while the catalytic effect of carbonic anhydrase on CO_2 hydration is a likely explanation for vital effects in coral $\delta^{18}O$.

8. CONCLUSIONS

We presented a new model for the oxygen isotope fractionation between $CaCO_3$ and water ($\alpha_{c/w}$) that includes kinetic isotope fractionations between $CaCO_3$ and CO_3^{2-} ions ($\alpha_{c/CO_3^{2-}}$) and between CO_3^{2-} ions and water ($\alpha_{CO_3^{2-}/w}$). In the model, CO_3^{2-} is the only precipitating DIC species while the other DIC species affect $\alpha_{c/w}$ via conversion to CO_3^{2-} shorty before or during $CaCO_3$ precipitation. The level of isotopic equilibration between $CaCO_3$ and CO_3^{2-} ions is expressed as a function of the solution Ω and ionic strength through the partial reaction order for CO_3^{2-} (Zhong and Mucci, 1993), while kinetic isotope fractionations between CO_3^{2-} and H_2O are calculated from the kinetics of CO_2 hydration and hydroxylation in water (Usdowski et al., 1991; Uchikawa and Zeebe, 2012). A comparison of modelled and measured $\alpha_{c/w}$ values leads to the following conclusions:

1. In solutions with low ionic strength ($I < 0.05$) and low CO_3^{2-}/Ca^{2+} activity ratio, $\alpha_{c/CO_3^{2-}}$ decreases from ~ 1.0054 to 1.0030 (~ 2.4‰ decrease in $^{18}O/^{16}O$) where the solution Ω increases from below ~ 1.6 to 12. These results indicate that oxygen isotope equilibration between $CaCO_3$ and the CO_3^{2-} pool is enhanced in solutions with low Ω and ionic strength such as the conditions of inorganic calcite formation within the Devils Hole cave system. In contrast, calcite or aragonite secreted by marine calcifiers is likely to form in conditions far from isotopic equilibrium because of high Ω and ionic strength in the organism's calcifying fluid.
2. The pH and mineral growth rate sensitivities of $\alpha_{c/w}$ depend on the level of isotopic equilibration between the precipitating CO_3^{2-} pool and water. When the precipitating CO_3^{2-} pool approaches isotopic equilibrium with water, small negative pH and/or growth effects on $\alpha_{c/w}$ occur because these parameters are positively correlated with Ω. This suggests that a pH dependence of $\alpha_{c/w}$ can arise even without any contribution of HCO_3^- ions to calcite growth. On the other hand, disequilibrium effects between CO_3^{2-} and H_2O can lead to strong positive or negative pH effects on $\alpha_{c/w}$ depending on the chemical

pathways antecedent to the production of CO_3^{2-} (e.g. CO_2 (de)hydration and (de)hydroxylation, HCO_3^- deprotonation).

3. Highly variable $\alpha_{c/w}$ values occur where the carbonate ion pool derives from gaseous CO_2 and the residence time of the DIC pool in solution is significantly shorter than the time required to reach DIC-H_2O isotopic equilibrium. These conditions make $\alpha_{c/w}$ sensitive to the $^{16}O/^{18}O$ of the CO_2 source and favour a strong negative correlation between $\alpha_{c/w}$ and pH due to the increasing contribution of oxygen atoms from OH^- ($^{18}O/^{16}O = -39‰$ relative to H_2O at 25 °C) to the precipitating DIC pool with increasing pH (i.e. increasing CO_2 hydroxylation rate) and the negative effect of pH on the rate of DIC-H_2O isotopic equilibration. Where the DIC derives from dissolved CO_2, the combined effect of pH on $CaCO_3$-CO_3^{2-} and CO_3^{2-}-H_2O fractionation leads to a maximum negative pH effect on $\alpha_{c/w}$ of $\sim 22‰$ at 25 °C. The effect of pH on $\alpha_{c/w}$ also decreases with increasing temperature.
4. The temperature dependence of $\alpha_{c/w}$ appears to originate from the effect of temperature on the $^{18}O/^{16}O$ of CO_3^{2-} in solution. This implies that isotopic disequilibrium effects between $CaCO_3$ and CO_3^{2-} should have little influence on the temperature dependence of $\alpha_{c/w}$. On the other hand, the temperature sensitivity of $\alpha_{c/w}$ is expected to deviate from $-0.22 \pm 0.02‰/°C$ (Kim and O'Neil, 1997) when the CO_3^{2-} pool does not reach isotopic equilibrium with water prior to $CaCO_3$ precipitation.
5. The $\delta^{18}O$ of foraminifers and corals can be explained by rapid and quantitative precipitation of internal DIC pools hosted in high-pH fluids. For planktic and benthic foraminifers, model results suggest that the DIC of the calcifying fluid is isotopically equilibrated at pH $\sim$ 8.8 prior to calcite precipitation. In contrast, coral $\delta^{18}O$ data is best explained by the precipitation of internal DIC derived from hydrated CO_2 and minimal subsequent DIC-H_2O isotopic equilibration. These models also show that the reduced and variable $\delta^{18}O$-temperature sensitivity of *Porites* coral aragonite (-0.11 to $-0.22‰/°C$) relative to that of foraminiferal calcite ($-0.21 \pm 0.01‰/°C$) can be explained by variable kinetic isotope effects associated to CO_2 hydration in the coral calcifying fluid.

ACKNOWLEDGEMENTS

E. Baker, M. Dietzel and J. Tang are thanked for sharing and explaining their valuable datasets. We are grateful to thoughtful input from R. Zeebe and A. Suzuki on early versions of this manuscript. We thank two anonymous reviewers for their valuable comments, which improved the manuscript. LSD was supported by a *University Postgraduate Award* from the University of Wollongong. JMW was supported by University of Oregon startup funds. HVM acknowledges support from Australian Research Council *Discovery Project* grant DP1092945 and from *Future Fellowship* FT140100286.

APPENDIX A

A.1. Notation

Symbol	Definition
DIC	Dissolved inorganic carbon
CA	Enzyme carbonic anhydrase
KIE	Kinetic isotope effect
KIF	Kinetic isotope fractionation
EIF	Equilibrium isotope fractionation
Ω	Solution saturation state with respect to a $CaCO_3$ mineral
K^*_{sp}	Stoichiometric solubility product of a $CaCO_3$ mineral
n_2	Partial reaction order for CO_3^{2-} during $CaCO_3$ precipitation
I	Ionic strength
r_{-c}	Rate of $CaCO_3$ dissolution (backward rate)
r_{+c}	Rate of $CaCO_3$ precipitation (forward rate)
r_c	Net rate of $CaCO_3$ precipitation
E_c	Level of isotopic equilibration between $CaCO_3$ and CO_3^{2-}
E_{DIC}	Level of isotopic equilibration between DIC and water
RT_{DIC}	Residence time of DIC in solution
τ	Time constant
k_{cat}	Catalytic rate constant
K_M	Michaelis-Menten constant
$^{18}R_w$	$^{18}O/^{16}O$ ratio of water
$^{18}R_c$	$^{18}O/^{16}O$ ratio of $CaCO_3$
$^{18}R_{CO_3^{2-}}$	$^{18}O/^{16}O$ ratio of CO_3^{2-}
$^{18}R^{-5}_{CO_3^{2-}}$	Initial $^{18}O/^{16}O$ ratio of CO_3^{2-} ions derived from deprotonated HCO_3^-
$^{18}R_{HCO_3^-}$	$^{18}O/^{16}O$ ratio of HCO_3^-
$^{18}R_{CO_2}$	$^{18}O/^{16}O$ ratio of CO_2
$^{18}R_{DIC}$	$^{18}O/^{16}O$ ratio of DIC
$^{18}R_{(CO_3^{2-}+HCO_3^-)}$	$^{18}O/^{16}O$ ratio of CO_3^{2-}+HCO_3^-
$^{18}R_{(CO_2+w)}$	$^{18}O/^{16}O$ ratio of CO_2+H_2O
$^{18}R_{(CO_2+OH^-)}$	$^{18}O/^{16}O$ ratio of CO_2+OH^-
$\alpha_{c/w}$	Oxygen isotope fractionation between $CaCO_3$ and water
$\alpha^{eq}_{c/w}$	Equilibrium limit of $\alpha_{c/w}$
$\alpha_{c/CO_3^{2-}}$	Oxygen isotope fractionation between $CaCO_3$ and CO_3^{2-}
$\alpha^{eq}_{c/CO_3^{2-}}$	Equilibrium limit of $\alpha_{c/CO_3^{2-}}$
$\alpha^{+c}_{c/CO_3^{2-}}$	Kinetic limit of $\alpha_{c/CO_3^{2-}}$
$\alpha^{-5}_{CO_3^{2-}/HCO_3^-}$	Kinetic limit of the oxygen isotope fractionation between CO_3^{2-} and HCO_3^- during HCO_3^- deprotonation
$\alpha_{CO_3^{2-}/w}$	Oxygen isotope fractionation between CO_3^{2-} and water
$\alpha_{HCO_3^-/w}$	Oxygen isotope fractionation between HCO_3^- and water
$\alpha_{CO_2/w}$	Oxygen isotope fractionation between CO_2 and water
$\alpha_{(CO_3^{2-}+HCO_3^-)/w}$	Oxygen isotope fractionation between (CO_3^{2-} + HCO_3^-) and water

$\alpha^{+2}_{(CO_3^{2-}+HCO_3^-)/CO_2}$	Oxygen isotope fractionation between (CO_3^{2-} + HCO_3^-) and CO_2 following CO_2 hydration
$\alpha^{+4}_{(CO_3^{2-}+HCO_3^-)/CO_2}$	Oxygen isotope fractionation between (CO_3^{2-} + HCO_3^-) and CO_2 following CO_2 hydroxylation
$^{16}k_{+c}$	Rate coefficient of ^{16}O transfer from CO_3^{2-} to $CaCO_3$ during $CaCO_3$ precipitation
$^{18}k_{+c}$	Rate coefficient of ^{18}O transfer from CO_3^{2-} to $CaCO_3$ during $CaCO_3$ precipitation
$^{16}k_{-5}$	Rate coefficient of ^{16}O transfer from HCO_3^- to CO_3^{2-} during HCO_3^- deprotonation
$^{18}k_{-5}$	Rate coefficient of ^{18}O transfer between HCO_3^- and CO_3^{2-} during HCO_3^- deprotonation
$^{16}k_{+2}$	Rate coefficient of ^{16}O transfer from CO_2 to hydrated CO_2 (HCO_3^-+CO_3^{2-}) during CO_2 hydration
$^{18}k_{+2}$	Rate coefficient of ^{18}O transfer from CO_2 to hydrated CO_2 (HCO_3^-+CO_3^{2-}) during CO_2 hydration
$^{16}k_{+4}$	Rate coefficient of ^{16}O transfer from CO_2 to hydroxylated CO_2 (HCO_3^-+CO_3^{2-}) during CO_2 hydroxylation
$^{18}k_{+4}$	Rate coefficient of ^{18}O transfer from CO_2 to hydroxylated CO_2 (HCO_3^-+CO_3^{2-}) during CO_2 hydroxylation
X_{+2}	Relative proportion of the DIC pool derived from hydrated CO_2
X_{+4}	Relative proportion of the DIC pool derived from hydroxylated CO_2

A.2. List of chemical reaction considered in this study

$$Ca^{2+} + CO_3^{2-} \overset{k_{-c}}{\underset{k_{+c}}{\Longleftrightarrow}} CaCO_3 \quad \text{(A1)}$$

$$CO_3^{2-} + H^+ \overset{k_{-5}}{\underset{k_{+5}}{\Longleftrightarrow}} HCO_3^- \quad \text{(A2)}$$

$$CO_2 + H_2O \overset{k^*_{-2},}{\underset{k^*_{+2}}{\Longleftrightarrow}} H_2CO_3 \Longleftrightarrow HCO_3^- + H^+ \quad \text{(A3)}$$

$$CO_2 + OH^- \overset{k_{-4},}{\underset{k_{+4}}{\Longleftrightarrow}} HCO_3^- \quad \text{(A4)}$$

A.3. Calcite and aragonite stoichiometric solubility product K_{sp}^*

The K_{sp}^* of calcite and aragonite in seawater was determined by Mucci (1983) as a function of temperature (T in Kelvin) and salinity (S in g/kg).

Calcite:

$$K^*_{spc} = 10\text{^}(-171.9065 - 0.077993T + 2839.319/T + 71.595LOG(T) + (-0.77712 + 0.0028426T + 178.34/T)S^{1/2} - 0.07711S + 0.0041249S^{3/2}) \quad \text{(A5)}$$

Aragonite:

$$K^*_{spa} = 10\text{^}(-171.945 - 0.077993T + 2903.293/T + 71.595LOG(T) + (-0.068393 + 0.0017276T + 88.135/T)S^{1/2} - 0.10018S + 0.0059415S^{3/2}) \quad \text{(A6)}$$

A.4. Reaction rate constants for CO_2 hydration (k_{+2}) and hydroxylation (k_{+4})

The rate constant k_{+2} was determined by Johnson (1982) while k_{+4} was calculated by Zeebe and Wolf-Gladrow (2001) from the data of Johnson (1982) as a function of temperature (T in Kelvin):

$$k_{+2} = \exp(1246.98 - 6.19.10^4 T^{-1} - 183 \ln T) \quad \text{(A7)}$$

$$k_{+4} = 4.7 \times 10^7 . \exp(-23200/(8.314T)) \quad \text{(A8)}$$

A.5. The time constant τ

The time constant τ represents the rate of oxygen isotope equilibration between DIC species and H_2O. It is a function of the hydration and hydroxylation reaction kinetics (Usdowski et al., 1991; Uchikawa and Zeebe, 2012):

$$\tau^{-1} = \frac{1}{2} \cdot [k^*_{+2} + k_{+4}[OH^-]] \cdot \left[1 + \frac{[CO_2]}{[DIC] - [CO_2]} - \sqrt{1 + \frac{2}{3} \cdot \frac{[CO_2]}{[DIC] - [CO_2]} + \left(\frac{[CO_2]}{[DIC] - [CO_2]}\right)^2}\right] \quad \text{(A9)}$$

with

$$k^*_{+2} = k_{+2} + \frac{k_{Cat}}{K_M} \cdot [CA] \quad \text{(A10)}$$

where k^*_{+2} and k_{+4} are the forward reaction rate constants for CO_2 hydration and hydroxylation, respectively (the superscript * of k^*_{+2} denote the inclusion of the effect of carbonic anhydrase on the rate of CO_2 (de)hydration), k_{Cat} is the catalytic rate constant, K_M is the Michaelis–Menten constant and $[CA]$ is the concentration of carbonic anhydrase in solution (Uchikawa and Zeebe, 2012).

A.6. The relative abundances of DIC species

The carbonate species are related by the following forward and backward reactions:

$$CO_{2(g)} + H_2O \overset{K_0}{\Longleftrightarrow} CO_{2(aq)} + H_2O \overset{K_1}{\Longleftrightarrow} HCO_3^- + H^+ \overset{K_2}{\Longleftrightarrow} CO_3^{2-} + 2H^+ \quad \text{(A11)}$$

The DIC speciation is determined by the solution pH and the stoichiometric dissociation constants of carbonic acid K_1^* and K_2^* (the notation * denote stoichiometric constants), defined as follow:

$$K_1^* = \frac{[HCO_3^-][H^+]}{[CO_{2(aq)}]}; \quad pK_1^* = pH + log[CO_{2(aq)}] - log[HCO_3^-] \quad \text{(A12)}$$

$$K_2^* = \frac{[CO_3^{2-}][H^+]}{[HCO_3^-]}; \quad pK_2^* = pH + log[HCO_3^-] - log[CO_3^{2-}] \quad \text{(A13)}$$

where pK_1^* and pK_2^* are the negative $\log_{10}$ of the first and second dissociation constants of carbonic acid respectively.

Using Eqs. (A12) and (A13), the relative proportion X of the DIC species is expressed as follows:

$$X_{CO_3^{2-}} = \left(10^{(pK_1^*+pK_2^*-2pH)} + 10^{(pK_2^*-pH)} + 1\right)^{-1} \quad \text{(A14)}$$

$$X_{HCO_3^-} = 10^{pK_2^*-pH}.\left(10^{(pK_1^*+pK_2^*-2pH)} + 10^{(pK_2^*-pH)} + 1\right)^{-1} \quad \text{(A15)}$$

$$X_{CO_{2(aq)}} = \left(10^{(2pH-pK_1^*-pK_2^*)} + 10^{(pH-pK_1^*)} + 1\right)^{-1} \quad \text{(A16)}$$

The equilibrium constants pK_1^* and pK_2^* were measured by Millero et al. (2006) for salinities varying from 0 to 50 g/kg:

$$pK_1^* = 13.4191S^{0.5} + 0.0331\mathrm{S} - 5.33.10^{-5}S^2 - (530.123S^{0.5} + 6.103\mathrm{S})T^{-1} - 2.0695S^{0.5}\ln\ \mathrm{T} + pK_1^0 \quad \text{(A17)}$$

$$pK_2^* = 21.0894S^{0.5} + 0.1248S - 3.687.10^{-4}S^2 - (772.483S^{0.5} + 20.051S)T^{-1} - 3.3336S^{0.5} \times \ln T + pK_2^0 \quad \text{(A18)}$$

with S the salinity and T the temperature in Kelvin. The value of pK_1^0 and pK_2^0 in (A17) and (A18) is obtained from Harned and Scholes (1941) and Harned and Davis (1943):

$$pK_1^0 = 6320.813T^{-1} + 19.568224\ln T - 126.34048 \quad \text{(A19)}$$

$$pK_2^0 = 5143.692T^{-1} + 14.613358\ln T - 90.18333 \quad \text{(A20)}$$

A.7. Stoichiometric ion product of water K_w^*

The ion product of water is used to calculate [OH^-] in Eqs. (43) and (44). Its dependence on temperature and salinity was determined by DOE (1994):

$$\ln K_w^* = 148.96502 - 13847.26/T - 23.6521\ln T + (118.67/T - 5.977 + 1.0495\ln T)S^{1/2} - 0.011615S \quad \text{(A21)}$$

A.8. Uncertainties of calculated parameters

Lower and upper uncertainties of calculated parameters from multiple variables with associated uncertainties were calculated assuming no correlations between the different variables. Given a parameter P_i that is a function of n variables $x_1, \ldots, x_n$ we have:

$$P_i = f(x_1, \ldots, x_n) \quad \text{(A22)}$$

Then the lower uncertainty of P_i is given by:

$$-\sigma_{P_i} = \sqrt{(P_i - f(x_1 - \sigma_{x_1}, \ldots, x_n))^2 + \ldots + (P_i - f(x_1, \ldots, x_n - \sigma_{x_n}))^2} \quad \text{(A23)}$$

where $\sigma_{x_1}, \ldots, \sigma_{x_n}$ are the lower uncertainties of the $x_1, \ldots, x_n$ variables if $x_1, \ldots, x_n$ are positively correlated with P_i or the upper uncertainties of the $x_1, \ldots, x_n$ variables if $x_1, \ldots, x_n$ are negatively correlated with P_i.

Similarly, the upper uncertainty of P_i is given by:

$$+\sigma_{P_i} = \sqrt{(P_i - f(x_1 + \sigma_{x_1}, \ldots, x_n))^2 + \ldots + (P_i - f(x_1, \ldots, x_n + \sigma_{x_n}))^2} \quad \text{(A24)}$$

where $\sigma_{x_1}, \ldots, \sigma_{x_n}$ are the upper uncertainties of the $x_1, \ldots, x_n$ variables if $x_1, \ldots, x_n$ are positively correlated with P_i or the lower uncertainties of the $x_1, \ldots, x_n$ variables if $x_1, \ldots, x_n$ are negatively correlated with P_i.

REFERENCES

Adkins J. F., Boyle E. A., Curry W. B. and Lutringer A. (2003) Stable isotopes in deep-sea corals and a new mechanism for "vital effects". *Geochim. Cosmochim. Acta* **67**, 1129–1143.

Al-Horani F. A., Al-Moghrabi S. M. and de Beer D. (2003) The mechanism of calcification and its relation to photosynthesis and respiration in the scleractinian coral Galaxea fascicularis. *Mar. Biol.* **142**, 419–426.

Allison N. and Finch A. A. (2010a) The potential origins and palaeoenvironmental implications of high temporal resolution $\delta^{18}O$ heterogeneity in coral skeletons. *Geochim. Cosmochim. Acta* **74**, 5537–5548.

Allison N. and Finch A. A. (2010b) $\Delta^{11}B$, Sr, Mg and B in a modern Porites coral: the relationship between calcification site pH and skeletal chemistry. *Geochim. Cosmochim. Acta* **74**, 1790–1800.

Allison N., Cohen I., Finch A. A., Erez J. and Tudhope A. W. (2014) Corals concentrate dissolved inorganic carbon to facilitate calcification. *Nat. Commun.* **5**, 5741.

Baker E. B. (2015) *Carbon and Oxygen Isotope Fractionation in Laboratory-Precipitated Inorganic Calcite* MSc thesis. University of Oregon.

Barras C., Duplessy J. C., Geslin E., Michel E. and Jorissen F. J. (2010) Calibration of $\delta^{18}O$ of cultured benthic foraminiferal calcite as a function of temperature. *Biogeosciences* **7**, 1349–1356.

Beck W. C., Grossman E. L. and Morse J. W. (2005) Experimental studies of oxygen isotope fractionation in the carbonic acid system at 15 °C, 25 °C, and 40 °C. *Geochim. Cosmochim. Acta* **69**, 3493–3503.

Bemis B. E., Spero H. J., Bijma J. and Lea D. W. (1998) Reevaluation of the oxygen isotopic composition of planktonic foraminifera: experimental results and revised paleotemperature equations. *Paleoceanography* **13**, 150–160.

Bentov S., Brownlee C. and Erez J. (2009) The role of seawater endocytosis in the biomineralization process in calcareous foraminifera. *Proc. Natl. Acad. Sci. USA* **106**, 21500–21504.

Bertucci A., Moya A., Tambutté S., Allemand D., Supuran C. T. and Zoccola D. (2013) Carbonic anhydrases in anthozoan corals – a review. *Bioorg. Med. Chem. Lett.* **21**, 1437–1450.

Bigeleisen J. and Wolfsberg M. (1958) Theoretical and experimental aspects of isotope effects in chemical kinetics. *Adv. Chem. Phys.* **1**, 15–76.

Bots P., Benning L. G., Rodriguez-Blanco J.-D., Roncal-Herrero T. and Shaw S. (2012) Mechanistic insights into the crystallization of amorphous calcium carbonate (ACC). *Cryst. Growth Des.* **12**, 3806–3814.

Cai W.-J., Ma Y., Hopkinson B. M., Grottoli A. G., Warner M. E., Ding Q., Hu X., Yuan X., Schoepf V., Xu H., Han C., Melman T. F., Hoadley K. D., Pettay D. T., Matsui Y., Baumann J. H., Levas S., Ying Y. and Wang Y. (2016) Microelectrode characterization of coral daytime interior pH and carbonate chemistry. *Nat. Commun.* **7**, 11144.

Candelier Y., Minoletti F., Probert I. and Hermoso M. (2013) Temperature dependence of oxygen isotope fractionation in coccolith calcite: a culture and core top calibration of the genus Calcidiscus. *Geochim. Cosmochim. Acta* **100**, 264–281.

Chivas A. R., De Deckker P., Wang S. X. and Cali J. A. (2002) Oxygen-isotope systematics of the nektic ostracod *Australo-*

cypris robusta. In *The Ostracoda: Applications in Quaternary Research, Geophysical Monograph 131* (eds. J. A. Holmes and A. R. Chivas). American Geophysical Union, Washington, DC, pp. 301–313.

Clark I. D. and Lauriol B. (1992) Kinetic enrichment of stable isotopes in cryogenic calcites. *Geochim. Cosmochim. Acta* **102**, 217–228.

Clark I. D., Fontes J.-C. and Fritz P. (1992) Stable isotope disequilibria in travertine from high pH waters: laboratory investigations and field observations from Oman. *Geochim. Cosmochim. Acta* **56**, 2041–2050.

Coplen T. B., Kendall C. and Hopple J. (1983) Comparison of stable isotope reference samples. *Nature* **302**, 236–238.

Coplen T. B. (2007) Calibration of the calcite–water oxygen-isotope geothermometer at Devils Hole, Nevada, a natural laboratory. *Geochim. Cosmochim. Acta* **71**, 3948–3957.

Demichelis R., Raiteri P., Gale J. D., Quigley D. and Gebauer D. (2011) Stable prenucleation mineral clusters are liquid-like ionic polymers. *Nat. Commun.* **2**, 590.

de Nooijer L. J., Toyofuku T. and Kitazato H. (2009) Foraminifera promote calcification by elevating their intracellular pH. *Proc. Natl. Acad. Sci. USA* **106**, 15374–15378.

DePaolo D. J. (2011) Surface kinetic model for isotopic and trace element fractionation during precipitation of calcite from aqueous solutions. *Geochim. Cosmochim. Acta* **75**, 1039–1056.

Devriendt L. S., McGregor H. V. and Chivas A. R. (2017) Ostracod calcite records the $^{18}O/^{16}O$ ratio of the bicarbonate and carbonate ions in water. *Geochim. Cosmochim. Acta*. http://dx.doi.org/10.1016/j.gca.2017.06.044.

Dietzel M., Usdowski E. and Hoefs J. (1992) Chemical and $^{13}C/^{12}C$- and $^{18}O/^{16}O$-isotope evolution of alkaline drainage waters and the precipiation of calcite. *Appl. Geochem.* **7**, 177–184.

Dietzel M., Tang J., Leis A. and Köhler S. J. (2009) Oxygen isotopic fractionation during inorganic calcite precipitation – effects of temperature, precipitation rate and pH. *Chem. Geol.* **268**, 107–115.

Dietzel, M., Purgstaller, B., Mavromatis, V., Immenhauser, A., Leis, A., Kluge, T., 2015. Transformation of Mg bearing ACC to Mg-calcite traced by $^{18}O/^{16}O$ and clumped isotopes. Goldschmidt 2015 Abtract.

DOE (1994) Handbook of methods for the analysis of the various parameters of the carbon dioxide system in seawater; version 2. ORNL/CDIAC.

Emiliani C. (1966) Paleotemperature analysis of Caribbean cores P6304–8 and P6304–9 and a generalized temperature curve for the past 425,000 years. *J. Geol.* **74**, 109–124.

Falk E. S., Guo W., Paukert A. N., Matter J. M., Mervine E. M. and Kelemen P. B. (2016) Controls on the stable isotope composition of travertine from hyperalkaline springs in Oman: insights from clumped isotope measurments. *Geochim. Cosmochim. Acta* **192**, 1–28.

Felis T., Patzold J. and Loya Y. (2003) Mean oxygen-isotope signatures in Porites spp. corals: inter-colony variability and correction for extension-rate effects. *Coral Reefs* **22**, 328–336.

Felis T., Lohmann G., Kuhnert H., Lorenz S. J., Scholz D., Patzold J., Al-Rousan S. A. and Al-Moghrabi S. M. (2004) Increased seasonality in Middle East temperatures during the last interglacial period. *Nature* **429**, 164–168.

Foster G. L. and Rae J. W. B. (2016) Reconstructing Ocean pH with Boron Isotopes in Foraminifera. *Annu. Rev. Earth Planet. Sci.* **44**, 207–237.

Gabitov R. I., Watson E. B. and Sadekov A. (2012) Oxygen isotope fractionation between calcite and fluid as a function of growth rate and temperature: an in situ study. *Chem. Geol.* **306–307**, 92–102.

Gagan M. K., Dunbar G. B. and Suzuki A. (2012) The effect of skeletal mass accumulation in *Porites* on coral Sr/Ca and ^{18}O paleothermometry. *Paleoceanography*.

Green M. and Taube H. (1963) Isotopic fractionation in the OH–H_2O exchange reaction. *J. Phys. Chem.* **67**, 1565–1566.

Harned H. S. and Scholes S. R. (1941) The ionization constant of HCO_3 from 0 to 50 °C. *J. Am. Chem. Soc.* **63**, 1706–1709.

Harned H. and Davis R. (1943) The ionization constant of carbonic acid in water and the solubility of carbon dioxide in water and aqueous salt solutions from 0 to 50 °C. *J. Am. Chem. Soc.* **65**, 2030–2037.

Hayes J. M. (1982) Fractionation et al.: an introduction to isotopic measurements and terminology. *Spectra* **8**, 3–8.

Hays J. D., Imbrie J. and Shackleton N. J. (1976) Variations in the Earth's orbit: pacemaker of the ice ages. *Science* **194**, 1121–1132.

Hendy C. (1971) The isotopic geochemistry of speleothemsI. The calculation of the effects of different modes of formation on the isotopic composition of speleothems and their applicability as paleoclimatic indicators. *Geochim. Cosmochim. Acta* **35**, 801–824.

Hermoso M., Minoletti F., Aloisi G., Bonifacie M., McClelland H. L. O., Labourdette N., Renforth P., Chaduteau C. and Rickaby R. E. M. (2016) An explanation for the ^{18}O excess in Noelaerhabdaceae coccolith calcite. *Geochim. Cosmochim. Acta* **189**, 132–142.

Hofmann A. E., Bourg I. C. and DePaolo D. J. (2012) Ion desolvation as a mechanism for kinetic isotope fractionation in aqueous systems. *Proc. Natl. Acad. Sci. USA* **109**, 18689–18694.

Hopkinson B. M., Tansik A. L. and Fitt W. K. (2015) Internal carbonic anhydrase activity in the tissue of scleractinian corals is sufficient to support proposed roles in photosynthesis and calcification. *J. Exp. Biol.* **218**, 2039–2048.

Jorgensen B. B., Erez J., Revsbech N. P. and Cohen Y. (1985) Symbiotic photosynthesis in a planktonic foraminiferan, *Globigerinoides sacculifer* (Brady), studied with microelectrodes. *Limnol. Oceanogr.* **30**, 1253–1267.

Johnson K. S. (1982) Carbon dioxide hydration and dehydration kinetics in seawater. *Limnol. Oceanogr.* **27**, 849–855.

Kim S.-T. and O'Neil J. R. (1997) Equilibrium and nonequilibrium oxygen isotope effects in synthetic carbonates. *Geochim. Cosmochim. Acta* **61**, 3461–3475.

Kim S.-T., Hillaire-Marcel C. and Mucci A. (2006) Mechanisms of equilibrium and kinetic oxygen isotope effects in synthetic aragonite at 25 °C. *Geochim. Cosmochim. Acta* **70**, 5790–5801.

Kim S.-T., O'Neil J. R., Hillaire-Marcel C. and Mucci A. (2007) Oxygen isotope fractionation between synthetic aragonite and water: influence of temperature and Mg^{2+} concentration. *Geochim. Cosmochim. Acta* **71**, 4704–4715.

Kim S.-T., Gebbinck C. K., Mucci A. and Coplen T. B. (2014) Oxygen isotope systematics in the aragonite–CO_2–H_2O–NaCl system up to 0.7 mol/kg ionic strength at 25 °C. *Geochim. Cosmochim. Acta* **137**, 147–158.

Kluge T., Affek H. P., Dublyansky Y. and Spötl C. (2014) Devils Hole paleotemperatures and implications for oxygen isotope equilibrium fractionation. *Earth Planet. Sci. Lett.* **400**, 251–260.

Köhler-Rink S. and Kühl M. (2005) The chemical microenvironment of the symbiotic planktonic foraminifer *Orbulina universa*. *Mar. Biol. Res.* **1**, 68–78.

Kosednar-Legenstein B., Dietztel M., Leis A. and Stingl K. (2008) Stable carbon and oxygen isotope investigation in historical lime mortar plaster – results from field and experimental study. *Appl. Geochem.* **23**, 2425–2437.

Krishnamurthy R. V., Schmitt D., Atekwana E. A. and Baskaran M. (2003) Isotopic investigation of carbonate growth on concrete structures. *Appl. Geochem.* **18**, 435–444.

Lasaga, A.C., 1981. Rate laws of chemical reactions. In: Lasaga, A. C., Kirkpatrick, R.J. (Eds.), Kinetics of Geochemical Processes. Rev. Mineral. pp. 1–68. Mineral. Soc. Amer.

Lopez O., Zuddas P. and Faivre D. (2009) The influence of temperature and seawater composition on calcite crystal growth mechanisms and kinetics: implications for Mg incorporation in calcite lattice. *Geochim. Cosmochim. Acta* **73**, 337–347.

Macleod G., Fallick A. E. and Hall A. J. (1991) The mechanism of carbonate growth on concrete structures, as elucidated by carbon and oxygen isotope analyses. *Chem. Geol.* **86**, 335–343.

Marchitto T. M., Curry W. B., Lynch-Stieglitz J., Bryan S. P., Cobb K. M. and Lund D. C. (2014) Improved oxygen isotope temperature calibrations for cosmopolitan benthic foraminifera. *Geochim. Cosmochim. Acta* **130**, 1–11.

McConnaughey T. (1989a) ^{13}C and ^{18}O isotopic disequilibrium in biological carbonates: I. Patterns. *Geochim. Cosmochim. Acta* **53**, 151–162.

McConnaughey T. (1989b) ^{13}C and ^{18}O isotopic disequilibrium in biological carbonates: II. In vitro simulation of kinetic isotope effects. *Geochim. Cosmochim. Acta* **53**, 163–171.

McCrea J. M. (1950) On the isotopic chemistry of carbonates and a paleotemperature scale. *J. Chem. Phys.* **18**, 849–857.

McCulloch M., Falter J., Trotter J. and Montagna P. (2012) Coral resilience to ocean acidification and global warming through pH up-regulation. *Nat. Clim. Change* **2**, 623–627.

Millero F. J., Graham T. B., Huang F., Bustos-Serrano H. and Pierrot D. (2006) Dissociation constants of carbonic acid in seawater as a function of salinity and temperature. *Mar. Chem.* **100**, 80–94.

Mucci A. (1983) The solubility of calcite and aragonite in seawater at various salinities. *Am. J. Sci.* **289**, 780–799.

Nebel H., Neumann M., Mayer C. and Epple M. (2008) On the structure of amorphous calcium carbonate—a detailed study by solid-state NMR spectroscopy. *Inorg. Chem.* **47**, 7874–7879.

Nielsen L., DePaolo D. and DeYoreo J. (2012) Self-consistent ion-by-ion growth model for kinetic isotopic fractionation during calcite precipitation. *Geochim. Cosmochim. Acta* **86**, 166–181.

Omata T., Suzuki A., Sato T., Minoshima K., Nomaru E., Murakami A., Murayama S., Kawahata H. and Maruyama T. (2008) Effect of photosynthetic light dosage on carbon isotope composition in the coral skeleton: long-term culture of *Porites* spp. *J. Geophys. Res.* **113**, G02014. http://dx.doi.org/10.1029/2007JG000431.

O'Neil J. R., Clayton R. N. and Mayeda T. K. (1969) Oxygen isotope fractionation in divalent metal carbonates. *J. Chem. Phys.* **51**, 5547–5558.

Rayleigh J. W. S. (1896) Theoretical considerations respecting the separation of gases by diffusion and similar processes. *Phil. Mag., Ser.* **5**(42), 493–498.

Rink S., Kuhl M., Bijma J. and Spero H. J. (1998) Microsensor studies of photosynthesis and respiration in the symbiotic foraminifer *Orbulina universa*. *Mar. Biol.* **131**, 583–595.

Rollion-Bard C., Chaussidon M. and France-Lanord C. (2003) PH control on oxygen isotopic composition of symbiotic corals. *Earth Planet. Sci. Lett.* **215**, 275–288.

Rollion-Bard C., Chaussidon M. and France-Lanord C. (2011) Biological control of internal pH in scleractinian corals: implications on paleo-pH and paleo-temperature reconstructions. *C.R. Geosci.* **343**, 397–405.

Rollion-Bard C., Saulnier S., Vigier N., Schumacher A., Chaussidon M. and Lécuyer C. (2016) Variability in magnesium, carbon and oxygen isotope compositions of brachiopod shells: implications for paleoceanographic studies. *Chem. Geol.* **423**, 49–60.

Saenger C., Affek H. P., Felis T., Thiagarajan N., Lough J. M. and Holcomb M. (2012) Carbonate clumped isotope variability in shallow water corals: temperature dependence and growth-related vital effects. *Geochim. Cosmochim. Acta* **99**, 224–242.

Shackleton N. (1967) Oxygen isotope analyses and Pleistocene temperatures re-assessed. *Nature* **215**, 15–17.

Siddall M., Rohling E. J., Almogi-Labin A., Hemleben C., Meischner D., Schmelzer I. and Smeed D. A. (2003) Sea-level fluctuations during the last glacial cycle. *Nature* **423**, 853–858.

Spero H. J., Bijma J., Lea D. W. and Bemis B. E. (1997) Effect of seawater carbonate concentration on foraminiferal carbon and oxygen isotopes. *Nature* **390**, 497–500.

Suzuki A., Hibino K., Iwase A. and Kawahata H. (2005) Intercolony variability of skeletal oxygen and carbon isotope signatures of cultured Porites corals: temperature-controlled experiments. *Geochim. Cosmochim. Acta* **69**, 4453–4462.

Tambutté S., Tambutté E., Zoccola D., Caminiti N., Lotto S., Moya A., Allemand D. and Adkins J. (2007) Characterization and role of carbonic anhydrase in the calcification process of the azooxanthellate coral Tubastrea aurea. *Mar. Biol.* **151**, 71–83.

Tudhope A. W., Chilcott C. P., McCulloch M. T., Cook E. R., Chappell J., Ellam R. M., Lea D. W., Lough J. M. and Shimmield G. B. (2001) Variability in the El Niño-Southern Oscillation through a glacial-interglacial cycle. *Science* **291**, 1511–1517.

Uchikawa J. and Zeebe R. E. (2012) The effect of carbonic anhydrase on the kinetics and equilibrium of the oxygen isotope exchange in the CO_2-H_2O system: implications for ^{18}O vital effects in biogenic carbonates. *Geochim. Cosmochim. Acta* **95**, 15–34.

Urey H. C. (1947) The thermodynamic properties of isotopic substances. *J. Chem. Soc.*, 562–581.

Usdowski E. and Hoefs J. (1990) Kinetic $^{13}C/^{12}C$ and $^{18}O/^{16}O$ effects upon dissolution and outgassing of CO_2 in the system CO_2-H_2O. *Chem. Geol.* **80**, 109–118.

Usdowski E., Michaelis J., Bottcher M. E. and Hoefs J. (1991) Factors for the oxygen isotope equilibrium fractionation between aqueous and gaseous CO_2, carbonic acid, bicarbonate, carbonate, and water (19 °C). *Z. Phys. Chem.* **170**, 237–249.

Venn A., Tambutté E., Holcomb M., Allemand D. and Tambutté S. (2011) Live tissue imaging shows reef corals elevate pH under their calcifying tissue relative to seawater. *PLoS ONE* **6**, e20013.

von Grafenstein U., Erlernkeuser H. and Trimborn P. (1999) Oxygen and carbon isotopes in modern fresh-water ostracod valves: assessing vital offsets and autecological effects of interest for palaeoclimate studies. *Palaeogeogr., Palaeoclimatol., Palaeoecol.* **148**, 133–152.

Wang Y. J., Cheng H., Edwards R. L., An Z. S., Wu J. Y., Shen C. C. and Dorale J. A. (2001) A high-resolution absolute-dated Late Pleistocene monsoon record from Hulu Cave, China. *Science* **294**, 2345–2348.

Wang Z., Gaetani G., Liu C. and Cohen A. (2013) Oxygen isotope fractionation between aragonite and seawater: developing a novel kinetic oxygen isotope fractionation model. *Geochim. Cosmochim. Acta* **117**, 232–251.

Watkins J. M., Nielsen L. C., Ryerson F. J. and DePaolo D. J. (2013) The influence of kinetics on the oxygen isotope composition of calcium carbonate. *Earth Planet. Sci. Lett.* **375**, 349–360.

Watkins J. M., Hunt J. D., Ryerson F. J. and DePaolo D. J. (2014) The influence of temperature, pH, and growth rate on the ^{18}O

composition of inorganically precipitated calcite. *Earth Planet. Sci. Lett.* **404**, 332–343.

Watkins J. M., DePaolo D. J. and Watson E. B. (2017) Kinetic fractionation of non-traditional stable isotopes by diffusion and crystal growth reactions. *Rev. Mineral. Geochem.* **82**, 85–125.

Watson E. B. (2004) A conceptual model for near-surface kinetic controls on the trace-element and stable isotope composition of abiogenic calcite crystals. *Geochim. Cosmochim. Acta* **68**, 1473–1488.

Winograd I. J., Coplen T. B., Landwehr J. M., Riggs A. C., Ludwig K. R., Szabo B. J., Kolesar P. T. and Revesz K. M. (1992) Continuous 500,000-year climate record from vein calcite in Devils Hole, Nevada. *Science* **258**, 255–260.

Wolthers M., Nehrke G., Gustafsson J. P. and Van Cappellen P. (2012) Calcite growth kinetics: modeling the effect of solution stoichiometry. *Geochim. Cosmochim. Acta* **77**, 121–134.

Wong C. and Breecker D. O. (2015) Advancements in the use of speleothems as climate archives. *Quat. Sci. Rev.* **127**, 1–18.

Xia J., Ito E. and Engstrom D. R. (1997) Geochemistry of ostracode calcite: Part 1. An experimental determination of oxygen isotope fractionation. *Geochim. Cosmochim. Acta* **61**, 377–382.

Zeebe R. E. (1999) An explanation of the effect of seawater carbonate concentration on foraminiferal oxygen isotopes. *Geochim. Cosmochim. Acta* **63**, 2001–2007.

Zeebe R. E. and Wolf-Gladrow D. (2001) *CO_2 in Seawater: Equilibrium, Kinetics, Isotopes*. Elsevier, Amsterdam.

Zeebe R. E. (2014) Kinetic fractionation of carbon and oxygen isotopes during hydration of carbon dioxide. *Geochim. Cosmochim. Acta* **139**, 540–552.

Zhong S. and Mucci A. (1989) Calcite and aragonite precipitation from seawater solutions of various salinities: precipitation rates and overgrowth compositions. *Chem. Geol.* **78**, 283–299.

Zhong S. and Mucci A. (1993) Calcite precipitation in seawater using a constant addition technique: a new overall reaction kinetic expression. *Geochim. Cosmochim. Acta* **57**, 1409–1417.

Ziveri P., Thoms S., Probert I., Geisen M. and Langer G. (2012) A universal carbonate ion effect on stable oxygen isotope ratios in unicellular planktonic calcifying organisms. *Biogeosciences* **9**, 1025–1032.

Zuddas P. and Mucci A. (1994) Kinetics of calcite precipitation from seawater: I. A classical chemical kinetics description for strong electrolyte solutions. *Geochim. Cosmochim. Acta* **58**, 4353–4362.

Zuddas P. and Mucci A. (1998) Kinetics of calcite precipitation from seawater: II. The influence of the ionic strength. *Geochim. Cosmochim. Acta* **62**, 757–766.

Associate Editor: Ruth Blake